Doctoral Dissertation

Studies on Synthesis and Properties of Alkali Metal and Nickel Complexes Bearing a Phenalenyl-Based Tridentate Ligand

Hikaru Noguchi

January 2025

Department of Applied Chemistry,
Graduate School of Engineering,
Osaka University

Preface and Acknowledgement

The research presented in this thesis was carried out under the direction of Professor Mamoru Tobisu of the Department of Applied Chemistry, Graduate School of Engineering, Osaka University. I was a student in Professor Nishimura's laboratory in Osaka City University (2022~now: Osaka Metropolitan University, OMU) from April 2019 to March 2020 and then moved to Professor Chatani's laboratory in Osaka University. I was a student in Chatani's laboratory from April 2020 to March 2022 and then moved to Professor Tobisu's laboratory. I was a student there from April 2022 to March 2025. The thesis is concerned with synthesis and properties of a T-shaped nickel metalloradical and corresponding nickel(II) and alkali metal complexes bearing a tridentate phenalenyl-based tridentate ligand.

This thesis could not have been completed without the support of numerous people. Here, I wish to express my sincerest appreciation to all of these people.

First, I express the utmost appreciation to Professor Mamoru Tobisu. His point of view made my thesis more fantastic and interesting for me. Under his guidance, my interest in chemistry glows up widely by much amazing advice to me. I also have great gratitude to him for very hard work for completion of my thesis: I always ask for help from professors who have the necessary skills and techniques. It makes me and my thesis more in-depth discussion I had never known. Therefore, I am very thankful to him for his advice and guidance.

Second, I wish to express my appreciation to Professor Naoto Chatani (current: Professor Emeritus of Osaka Univ.; Special Appointment Professor, Osaka Univ.). He encouraged me to advance to Ph.D. course. He did not say strong words, but his words broke my overthinking to Ph.D. course.

Third, I wish to express my appreciation to Associate Professor Yoshiya Fukumoto. His perspective on research and data is very deep and essential for scientists. In my two years in Chatani group, he taught me these points of view not only directly but also by my teaching to other students. It was a great opportunity for me to take my step towards a researcher.

I sincerely appreciate Assistant Professor Yusuke Ano (current position: Associate Professor, Kindai Univ.), Professor Hayato Tsurugi, Assistant Professor Hayato Fujimoto, Assistant Professor Takuya Kodama, Professor Takahiro Nishimura (the graduate school of science, OMU), Associate Professor Kazuhiko Sakaguchi (the graduate school of science, OMU) for instructive advice based on their profound understanding of chemistry.

I also express my appreciation to the secretaries in our laboratory, including Ms. Junko Ohmagari and Ms. Kyoko Kawashima for their generous assistance.

I also wish to express my appreciation to the past and present members of the Tobisu, Chatani, and Nishimura groups. The respectable and talented senior members: Dr. Yasuaki, Iyori (Chatani group), Dr. Chen-an Wang (Chatani group), Dr. Qiyuan He (Chatani group), Dr. Tomoki Yoshida (Tobisu group), Dr. Kana Sakamoto (Nishimura group), Dr. Ryoma Shimazumi (Tobisu group), Dr. Hisayasu Ishibashi (Chatani group), Mr. Natsuki

Kawai, Mr. Shizuki Monda, Mr. Itsuki Nohira, Ms. Nozomi Ohara (Chatani group), Mr. Shunnichi Kubota, Mr. Ikumi Nakamura, Mr. Shouma Ariyoshi, Ms. Kotone Murakami (Nishimura group). Thanks to them, my stay here was both fruitful and happy and it was able to advance my research through discussions with them.

I also wish to express my thanks to my colleagues in the Tobisu, Chatani, and Nishimura groups: Mr. Akihisa Matsuura (since 3rd grade of Osaka City Univ.), Ms, Yuka Okawa, Mr. Ryota Yabe (Nishimura group), Ms. Haruka Kawakami, Ms. Aoi Morishige, Mr. Daichi Takahashi, Mr. Tianhao Zhang (Chatani group). They were highly motivated, worked hard and inspired me.

I also wish to express my appreciation to the younger members of the Tobisu and Chatani groups: Ms. Sakura Takahashi (Chatani and Tobisu groups), Mr. Ryosuke Nagamure, Mr. Kumpei Nishimura, Mr. Tatsuya Hirano, Mr. Haruki Hirosawa, Mr. Yuuki Nakamoto, Mr. Kazumune Yo, Mr. Syunsuke Watanabe, Ms. Nami Tanaka, Mr. Shotaro Yano, Mr. Kippei Yamamura (Chatani group), Mr. Tetsuya Inagaki, Mr. Bunta Nakayasu, Mr. Satoshi Ogawa, Mr. Riku Tanimoto, Mr. Kenta Uchida, Mr. Takahiro Ando, Mr. Hiroki Morita, Mr. Nijito Mukai, Mr. Ryota Shiraki, Mr. Shisato Yamamura, Mr. Yuki Akita, Mr. Taiki Arima, Mr. Tomoya Enmei, Mr. Kazuya Imachi, Ms. Namiki Takenaka, Mr. Takayuki Enomoto, Ms. Moe Morimoto, Ms. Yui Morimoto, Mr. Teruki Nishioka, Mr. Tomoya Ueda, Mr. Sei Harada, Mr. Ibuki Hirai, Mr. Sota Iwasaki, Mr. Masayuki Mizutani, and Mr. Ryoichi Tabata (Tobisu group).

Furthermore, I wish to acknowledge the talented postdocs, Dr. Amrita Das, Dr. Sanjit Kumar Mahato, Dr. Shrikant Khake Manmathappa, Dr. Bernard Frederick Parker, Dr. Supriya Rej (Chatani group), Dr. Vishal Kumar Rawat, and Dr. Waroton Paisuwan (Tobisu group).

I also acknowledge Tsurugi group members to help me to handle my complexes: Mr. Takuya Akiyama, Mr. Sota Tamaki, Mr. Yu Kuroda, Mr. Tomohiro Mohri, Mr. Tao Kasahara, Mr. Eitaro, Mr. Yoshiki Imazato, Mr. Shunsuke Kimura, Mr. Yusuke Oda, Mr. Shuto Wakita, and Ms. Miyuki Takahama (as a secretary).

Lastly, I express my appreciation for my family; Ms. Kae Noguchi and Ms. Shigemi Noguchi for their continuous and generous support.

Suita, Osaka

January 2025

Hikaru Noguchi

Contents

General Introduction

Organic radicals have long served as crucial active species in organic synthesis.[1] In general, organic radicals possess an unpaired electron in their molecular orbitals derived from s or p orbitals. Examples include hydrogen atom and alkyl radicals, known as σ-radicals, which are not stabilized by π-conjugation. Radicals that are stabilized by π-conjugate systems, such as TEMPO and cyclopentadienyl, are categorized by π-radicals. Among organic radicals, carbon-centered radicals, which are generated by homolysis of weak covalent bonds or deprotonation of radical cations, are particularly important in organic synthesis. However, there are no examples of using carbon-centered radicals directly as catalysts in organic synthesis, due to the thermodynamic challenges associated with regenerating active species, as these radicals are often unstable (**Figure 1**).

Figure 1 Typical examples of organic radicals.

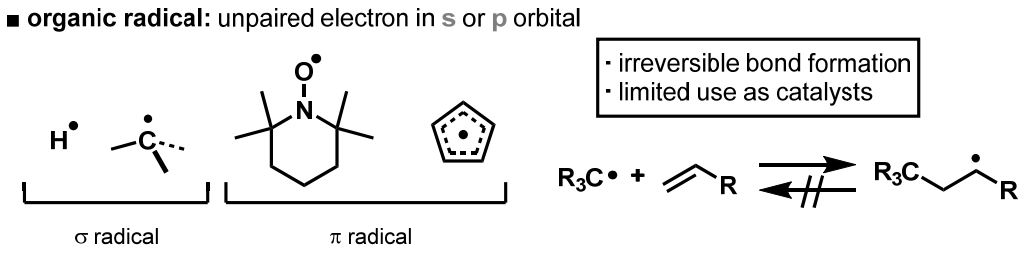

In contrast to organic radicals, transition metal complexes with an unpaired electron in their d orbitals, termed "metalloradicals", present unique opportunities. Metalloradicals can form unstable metal–carbon bonds or metal–heteroatom bonds with organic reactants, enabling them to act as radical catalysts by reversible bond formation and homolysis (**Figure 2**).[2]

Figure 2 Typical examples of metalloradicals.

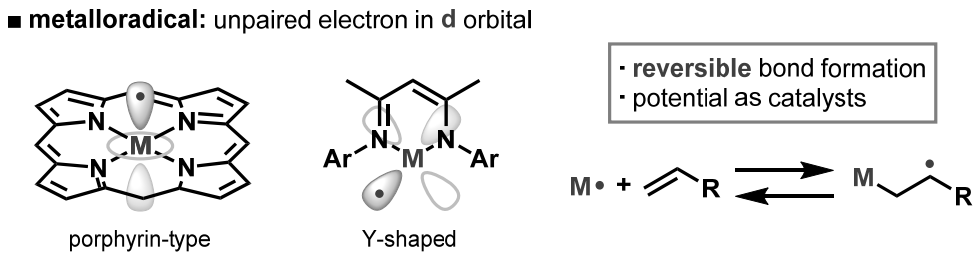

Metalloradicals can promote organic radical-like elementary reactions, such as homolytic cleavage of weak covalent bonds (*e.g.*, S–S bonds in disulfides), halogen or hydrogen abstraction, and addition to unsaturated molecules like ethylene or CO_2 (**Figure 3**). These reactivities contrast sharply with typical transition metal-mediated elementary reactions, such as oxidative addition/reductive elimination or migratory insertion/β-elimination, offering a pathway to unique catalytic cycles by combining both types of reactivities.

Figure 3 Typical reactivities of metalloradicals.

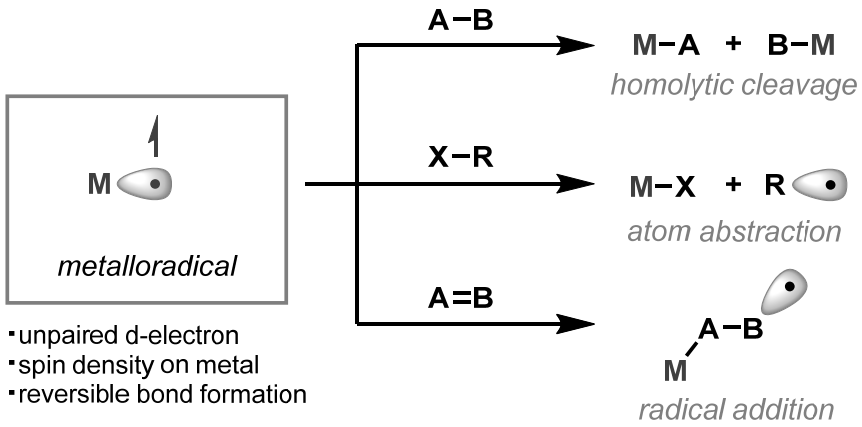

Metalloradicals play key roles in several catalytic transformations, especially in enzymatic processes.[3] For example, isomerization reactions involving hydrogen atom transfer (HAT) are catalyzed by cobalamins, which is a derivative of vitamin B_{12}.[3a] These reactions involve homolysis of the Co–C bond in a cobalamin derivative, facilitated by steric hinderance between alkyl group on cobalt and the ancillary ligand, to generate alkyl radicals and a Co(II) metalloradical intermediate. The generated alkyl radicals then participate in HAT to promote isomerization or undergo transition metal-invoived bimolecular homolytic substitution (S_H2)[4] reactions, as seen in enzymatic alkyl radical transfer (**Scheme 1**).

Scheme 1 Metalloradical catalysis in biological system.

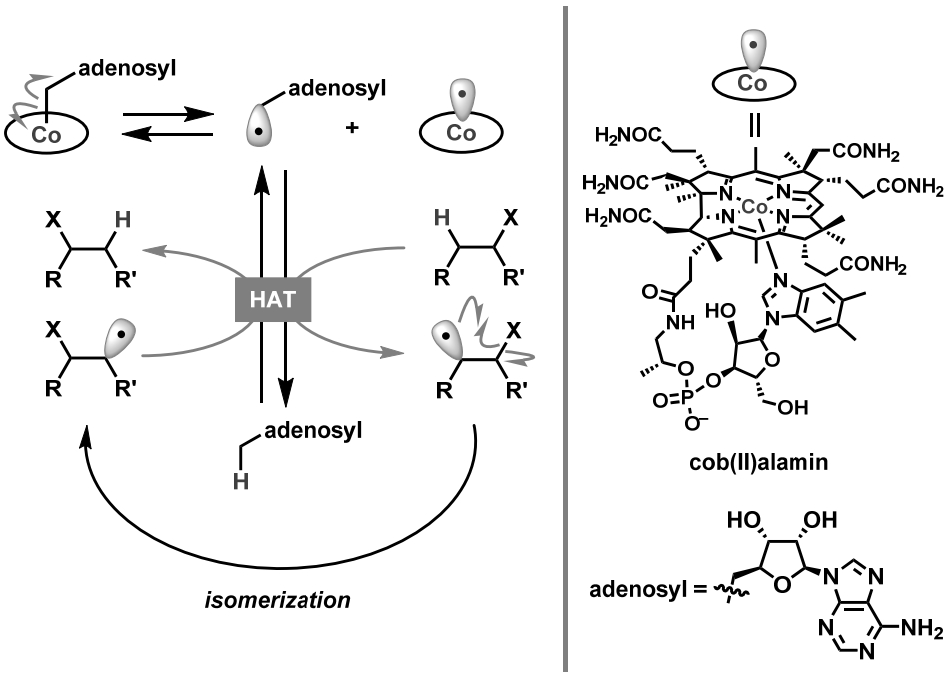

Beyond enzymatic reactions, porphyrin-based metalloradicals have been explored in catalytic organic synthesis. Zhang reported that cyclopropanation of alkenes using diazo compounds is catalyzed by a CoTPP (tetraphenylporphyrin) complex (**Scheme 2**).[5] In this reaction, a cobalt radical initially reacts with a diazo compound

to generate a cobalt-bound carbon-centered radical. The alkyl radical then adds to an alkene, followed by the S_H2 reaction to produce cyclopropane and regenerate the catalyst.

Scheme 2 Cyclopropanation of alkenes catalyzed by cobalt metalloradical.

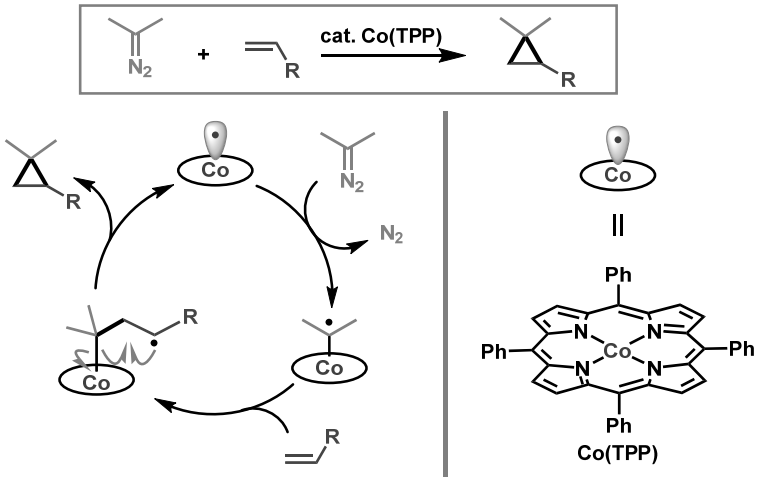

However, such metalloradical-catalyzed reactions (MRC) remain largely limited to porphyrin-based systems, whose synthesis and functionalization present significant challenges, thus narrowing their versatility.[6]

Recently, *in situ* generated metalloradicals from stable transition metal complexes have been employed in catalytic transformations, such as the nickel-catalyzed isomerization of vinylcyclopropanes reported by Schoenebeck (**Scheme 3**).[7] DFT studies suggested that a monomeric nickel(I) complex generated from nickel dimer plays a key role in this catalytic cycle. This reaction highlights the features of metalloradicals, including addition to an unsaturated bond and homolytic cleavage of a metal–carbon bond. While similar reactions were reported using stable thiyl radicals as catalysts,[8] this was the first report utilizing a metalloradical for such transformations. Although several other successful examples based on *in situ* generated approaches have been reported,[7,9] the authors sought to develop new metalloradicals that could be directly applied in catalytic reactions.

Scheme 3 Isomerization of vinylcyclopropanes catalyzed by nickel metalloradical.

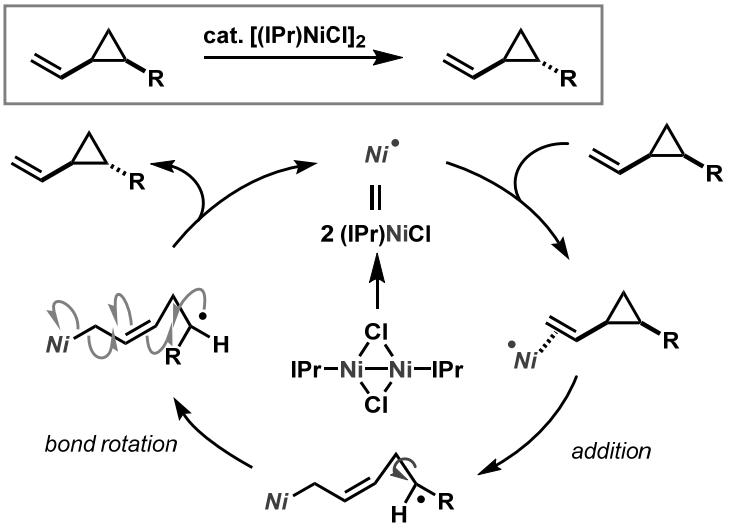

Metalloradicals can be classified into four types: porhyrin-based,[2a] T-shaped,[2b] Y-shaped,[2c,10] and linear[11] metalloradicals (**Figure 4**).[12]. These geometries influence the ligand field splitting of their d orbitals, typically resulting in a low-spin state with an unpaired electron. When the metal center has an odd number of electrons, it can behave as a metalloradical. For example, d^7 porphyrin complexes (*cf.* Co(TPP) etc.) have a destabilized d_{z^2} orbital, which is σ-symmetric and perpendicular to the porphyrin plane, as a singly occupied molecular orbital (SOMO) (**Figure 5**, left). Similarly, in the case of d^9 T-shaped metalloradicals, the $d_{x^2-y^2}$ orbital is destabilized to serve as the SOMO with σ-symmetry. However, unlike the porphyrin-based complexes, the SOMO is coplanar to ligand plane, which could facilitate the control of the metal center's reactivity by the substituents on the nitrogen atoms in the ligand (**Figure 5**, center). In contrast, d^9 Y-shaped metalloradicals have a destabilized d_{xy} orbital, which is π-symmetric, as a SOMO (**Figure 5**, right). We envisioned that, among these, T-shaped complexes with their σ-symmetric SOMO are particularly promising for the formation of new σ-bonds, a critical step for diverse catalytic applications.

Figure 4 Typical structures of metalloradicals.

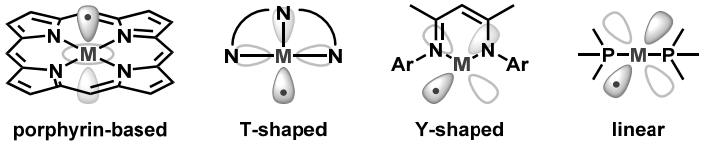

Figure 5 Typical ligand field splitting of metalloradicals.

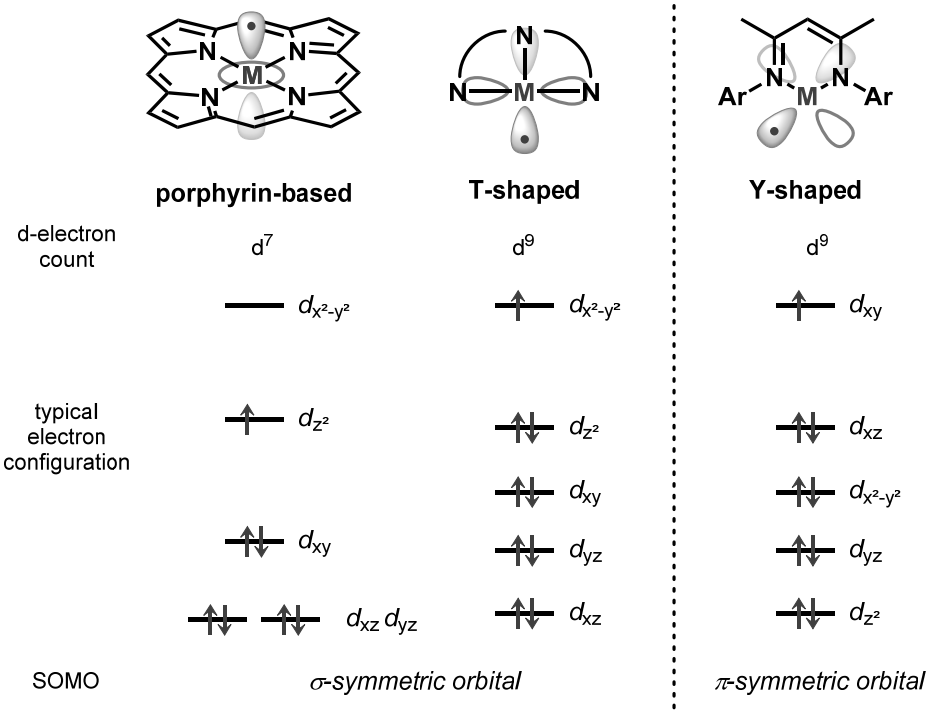

In **Figure 6**,[13] reported T-shaped nickel metalloradicals are summarized. Holland[13a] reported that the nickel complex with a bidentate NacNac ligand and carbon monoxide behaves as a T-shaped metalloradical, indicating that both σ-donating and π-accepting properties are important for creating T-shaped metalloradicals. Later, Caulton[13b] reported a

T-shaped metalloradical bearing a monoanionic P,N,P-tridentate ligand, which bears σ-donating amide and π-accepting phosphine moieties. Recently, Sen[13h] has reported a T-shaped nickel metalloradical bearing a NacNac-based tridentate ligand.

Figure 6 Reported T-shaped nickel metalloradicals.

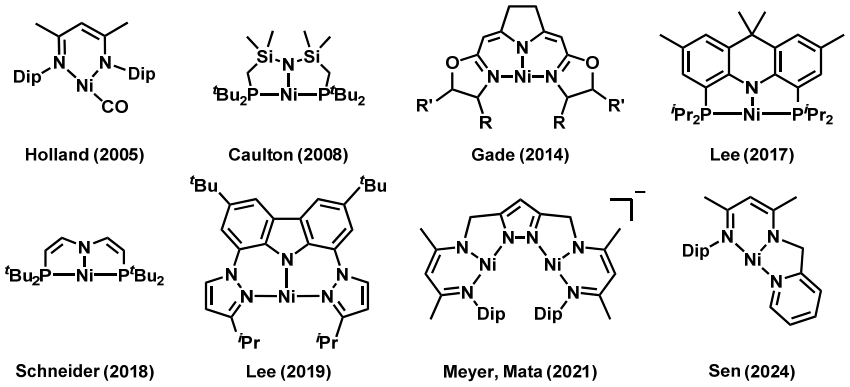

As for the catalytic application of these metalloradicals, Gade reported hydrodehalogenation of *gem*-dihaloalkanes (**Scheme 4**).[13c,14] In this reaction, hydride reagents did not reduce *gem*-dihaloalkanes directly but instead reduce Ni–X bonds, generated via halogen abstraction by the nickel metalloradical from the *gem*-dihaloalkanes. However, the potential of T-shaped nickel metalloradicals remains underexplored .

Scheme 4 Limited successful examples of T-shaped nickel metalloradical catalyzed reactions.

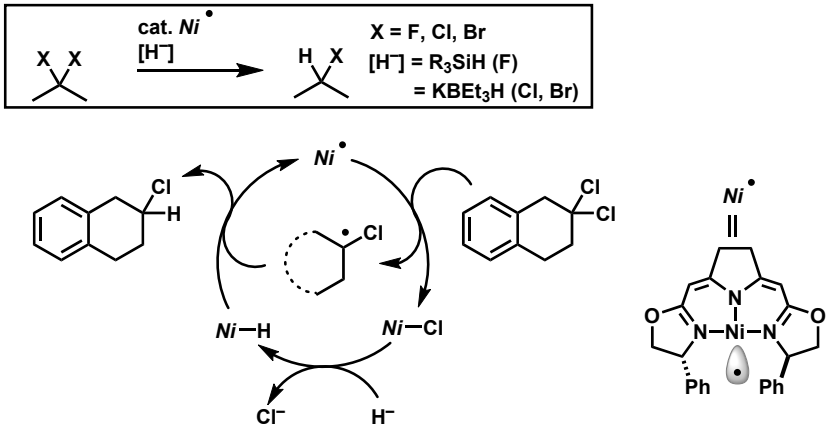

Our group, recently, reported low-valent main-group complexes bearing a phenalenyl(PLY)-based bidentate ligands.[15] PLY is a fused compound based on three benzenes and can stabilize radicals through resonance delocalization.[16] PLY-based bidentate ligands are one of the π-extended NacNac-based ligands and stable to radicals or anionic reactants due to less number of C(sp^3)–H bonds than NacNac-based ligands. The author envisioned that introducing 8-quinolyl moiety to the PLY-based ligand would lead to creating new PLY-based tridentate ligands with keeping the favorable features of the PLY-based bidentate ligands. In this thesis, the author reports the synthesis and properties of nickel metalloradicals and corresponding alkali metals and nickel(II) complexes bearing the PLY-based tridentate ligand (**Figure 7**).

Figure 7 Our previous works and this thesis work.

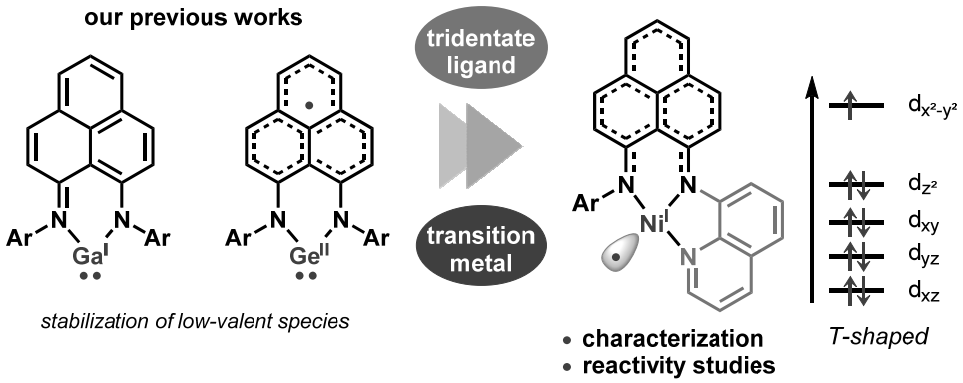

This thesis consists of the following three chapters (**Scheme 5**). In chapter 1, the author reports the synthesis of the ligand and its alkali metal salts. UV-vis spectroscopy and DFT studies reveal the origin of the colors in solution, depending on the alkali metals. In chapter 2, the author synthesized a nickel metalloradical using a NiBr precursor. UV-vis, XAFS, ESR measurements, and DFT studies revealed generation of a nickel metalloradical. The author also investigated the reactivities of the nickel metalloradical. In chapter 3, the author reports the synthesis of the nickel metalloradical by a different pathway from that reported in chapter 2. Using cationic nickel as a precursor was found to be more effective for synthesizing the nickel metalloradical.

Scheme 5 Contents of this thesis work.

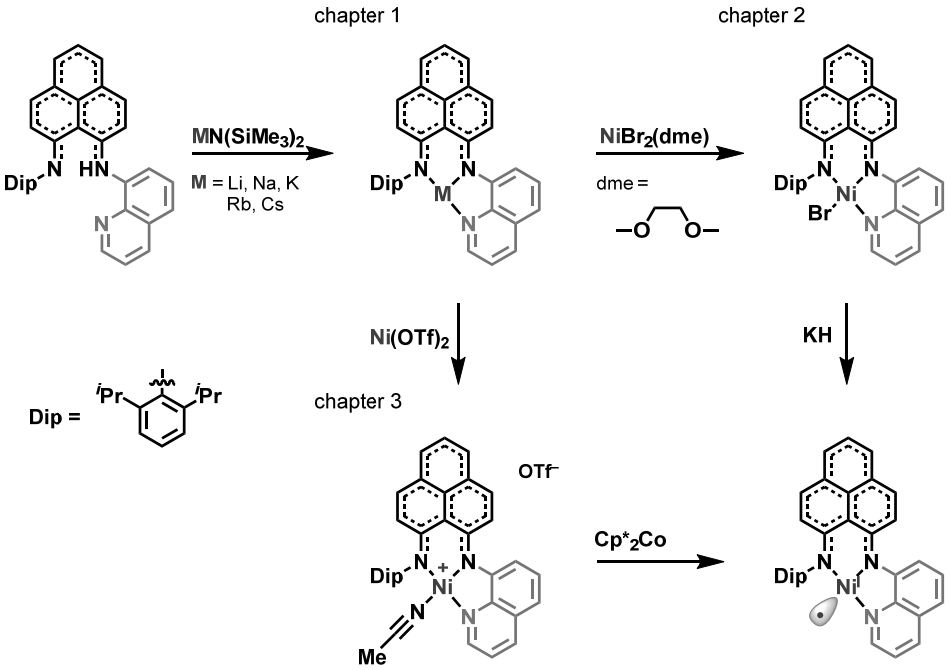

References

1. (a) Rowlands, G. J. *Tetrahedron* **2009**, *65*, 8603. (b) Rowlands, G. J. *Tetrahedron* **2010**, *66*, 1593. (c) Studer, A.; Curran, D. P. *Angew. Chem., Int. Ed.* **2016**, *55*, 58.

2. (a) Lee, W.-C. C.; Zhang, X. P. *Angew. Chem., Int. Ed*. **2024**, *63*, e202320243. (b) Ott, J. C.; Bürgy, D.; Guan, H.; Gade, L. H. *Acc. Chem. Res*. **2022**, *55*, 857. (c) Mindiola, D. J. *Angew. Chem., Int. Ed.* **2009**, *48*, 6198.

3. (a) Bridwell-Rabb, J.; Li, B.; Drennan, C. L. *ACS Bio Med Chem Au* **2022**, *2*, 173. (b) S. W. Ragsdale, *J. Biol. Chem.* **2009**, *284*, 18571.

4. (a) Nemoto, D. T. Jr.; Bian, K.-J.; Kao, S.-C.; West, J. G. *Beilstein J. Org. Chem.* **2023**, *19*, 1225. (b) Zhang, Y.; Li, K.-D.; Huang, H.-M. *ChemCatChem* **2024**, *16*, e202400955.

5. Lu, H.; Zhang, X. P. *Chem. Soc. Rev.* **2011**, *40*, 1899.

6. Senge, M. O.; Sergeeva, N. N.; Hale, K. J. *Chem. Soc. Rev.* **2021**, *50*, 4730.

7. Mendel, M.; Karl, T. M.; Hamm, J.; Kaldas, S. J.; Sperger, T.; Mondal, B.; Schoenebeck, F. *Nature* **2024**, *631*, 80.

8. (a) Dénes, F.; Pichowicz, M.; Povie, G.; Renaud, P. *Chem. Rev.* **2014**, *114*, 2587. (b) Subramanian, H.; Moorthy, R.; Sibi, M. P. *Angew. Chem., Int. Ed.* **2014**, *53*, 13660. (c) Patehebieke, Y. *Beilstein J. Org. Chem.* **2020**, *16*, 1418. (d) Xiao, W.; Wu, J. *ChemCatChem* **2023**, *15*, e202300541.

9. Light-induced homolysis of M–M bond. Mn: Jamatia, R.; Mondal, A.; Srimani, D *Adv. Synth. Catal*. **2021**, *363*, 2969.; Os: Lewandowska-Andralojc, A.; Grills, D. C.; Zhang, J.; Bullock, R. M.; Miyazawa, A.; Kawanishi, Y.; Fujita, E. *J. Am. Chem. Soc*. **2014**, *136*, 3572.

10. Tsai, Y.-C. *Coord. Chem. Rev.* **2012**, *256*, 722.

11. Noor, A. *Coord. Chem. Rev.* **2023**, *476*, 214941.

12. Few examples of other geometries.; trigonal bipyramidal: de Bruin, B.; Thewissen, S.; Yuen, T.-W.; Peters, T. P. J.; Smits, J. M. M.; Gal, A. W. *Organometallics* **2002**, *21*, 4312.; square planar (not porphyrin): Zovko, C.; Krätschmer, F.; Schmidt, S.; Seifert, T. P.; Gamer, M. T.; Roesky, P. W. *ChemPlusChem* **2022**, *87*, e202200288.; trigonal planar (*in situ* generated): Zhang, J.; Grills, D. C.; Huang, K.-W.; Fujita, E.; Bullock, R. M. *J. Am. Chem. Soc*. **2005**, *127*, 15684.

13. (a) Eckert, N. A.; Dinescu, A.; Cundari, T. R.; Holland, P. L. *Inorg. Chem*. **2005**, *44*, 7702. (b) Ingleson, M. J.; Fullmer, B. C.; Buschhorn, D. T.; Fan, H.; Pink, M.; Huffman, J. C.; Caulton, K. G.; *Inorg. Chem.* **2008**, *47*, 407. (c) Rettenmeier, C.; Wadepohl, H.; Gade, L. H. *Chem. Eur. J.* **2014**, *20*, 9657. (d) Yoo, C.; Lee, Y. *Angew. Chem., Int. Ed*. **2017**, *56*, 9502. (e) Schneck, F.; Ahrens, J.; Finger, M.; Stueckl, A. C.; Wuertele, C.; Schwarzer, D.; Schneider, S. *Nat. Commun.* **2018**, *9*, 1161. (f). Ghannam, J.; Sun, Z.; Cundari , T. R.; Zeller, M.; Lugosan, A.; Stanek, C. M.; Lee, W.-T. *Inorg. Chem*. **2019**, *58*, 7131. (g) Duan, P.-C.; Schulz, R. A.; Römer, A.; Van Kuiken, B. E.; Dechert, S.; Demeshko, S.; Cutsail III, G. E.; DeBeer, S.; Mata, R. A.; Meyer, F. *Angew. Chem., Int. Ed*. **2021**, *60*, 1891. (h) Pahar, S.; Sharma, V.; Raj, K. V.; Sangole, M. P.; George, C. P.; Singh, K.; Vanka, K.; Gonnade, R. G.; Sen, S. S. *Chem. Eur. J.* **2024**, *30*, e202303957.

14. (a) Wenz, J.; Rettenmeier, C. A.; Wadepohl, H.; Gade, L. H. *Chem. Commun.* **2016**, *52*, 202. (b) Rettenmeier, C. A.; Wenz, J.; Wadepohl, H.; Gade, L. H. *Inorg. Chem.* **2016**, *55*, 8214.

15. (a) Kodama, T.; Mukai, N.; Tobisu, M. *Inorg. Chem*. **2023**, *62*, 6554. (b) Kodama, T.; Uchida, K.; Nakasuji, C.; Kishi, R.; Kitagawa, Y.; Tobisu, M. *Inorg. Chem*. **2023**, *62*, 7861.

16. (a) Mukherjee, A.; Sau, S. C.; Mandal, S. K. *Acc. Chem. Res.* **2017**, *50*, 1679. (b) Ahmed, J.; Mandal, S. K. *Chem. Rev.* **2022**, *122*, 11369.

Chapter 1

Synthesis and Characterization of Alkali Metal Salts Bearing a Phenalenyl-Based Tridentate Ligand

1.1. Introduction

β-Diketiminate (NacNac)-based ligands are widely used for many main-group and transition metal complexes as a ligand with tunable kinetic stability and electronic structure (**Scheme 1**)[1] However, instabilities to radicals and anionic reagents and, which are caused by 1,3-diketone structure, are led to polymerization or decomposition of unstable complexes, such as low-valent complexes.

Scheme 1 NacNac-based complexes

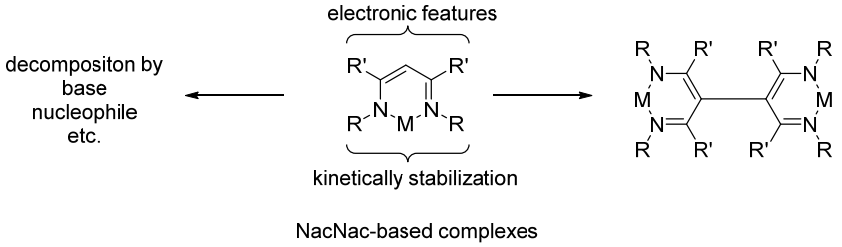

Recently, our group reported low-valent, main-group element complexes that bear a phenalenyl (PLY)-based bidentate ligand (**Scheme 2 left**)[2] which is π-extended NacNac-based ligand to increase stabilities to radicals and anionic reagents. For creating new types of N,N,N-tridentate ligand, the author attempted to replace one of the Dip (2,6-diisopropylphenyl) group to 8-quinolyl group (**Scheme 2 right**).[3] Herein the author report that synthesis of new PLY-based N,N,N-tridentate ligand and characterization of its alkali metal salts.

Scheme 2 (left) our previous works, (right) this work

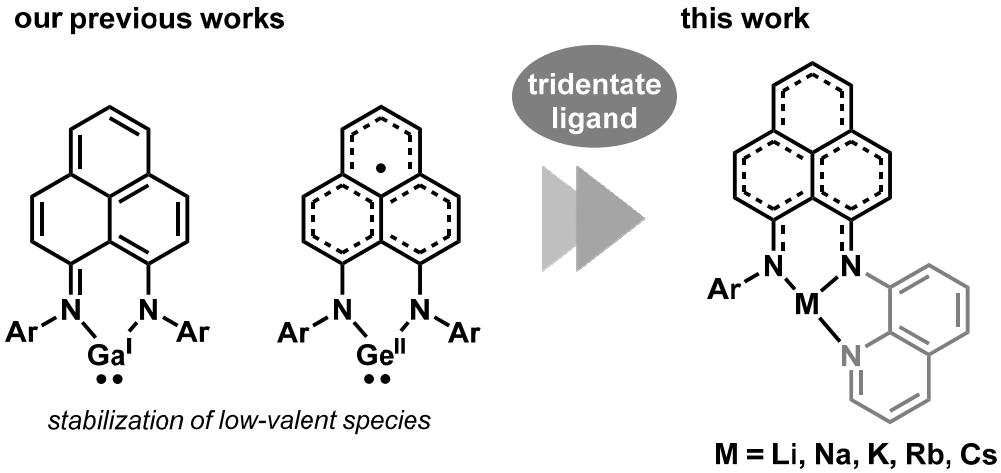

1.2. Results and Discussion

Initially, we synthesized a PLY-based tridentate ligand **1** bearing Dip and 8-quinolyl groups on nitrogen

atoms (**Scheme 3**). The synthesis involved O-methylation of **pre-1**[2b] with Meerwein reagent, which was followed by a reaction with lithium 8-quinolylamide to provide tridentate ligand **1**.[3] During synthetic trials of the alkali metal salts for the complexation to various transition metal (pseudo)halides, the author observed that the color of the toluene solution of the alkali metal salts **2a**–**2e** exhibited a bathochromic shift relative to the free ligand, with the degree of the shift varying depending on the alkali metal used.

Scheme 3 Synthetic scheme of alkali metal salts.

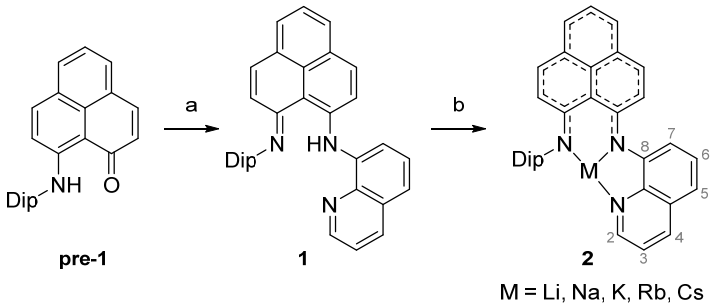

Reaction conditions; (a) Me_3OBF_4 (1.5 equiv), DCE, 15 h, then lithium 8-quinolylamide (2.0 equiv), THF, –78 °C to rt, 15 h, 32%. (b) for K salt: K-HMDS (1 M in THF, 1.2 equiv), THF, rt, 3 h; for other salts: M-HMDS (2 equiv for M = Na, 1 equiv for other metals), toluene-d_8, rt, immediately complexation. DCE: 1,2-dichroloethane.

^{1}H NMR spectra in toluene-d_8 revealed that the protons at the 2-position of the quinoline moieties in complexes **2a**–**2e** appear in the range of 8.13–7.70 ppm, whereas the corresponding proton in free ligand **1** appears at 8.54 ppm. This observation suggests that the electron density of the quinoline ring increased upon deprotonation (**Table 1**). The signal of these protons appeared as sharp doublets for **2a** and **2b**, as observed for **1**. In contrast, **2c**–**2e** displayed broad singlet. Polar solvents such as DMSO, DMF, and CH_3CN could not be used for ^{13}C NMR measurements because 2a to 2e readily deprotonate the acidic C–H bonds in these solvents.

Table 1 The ^{1}H NMR chemical shifts of the protons on the 2-position of quinoline moieties.[a]

	1	**2a**	**2b**	**2c**	**2d**	**2e**
δ/ppm	8.54	8.13	7.70	7.99	7.94	7.98
coupling	d	d	d	brs	brs	brs

[a]d: doublet; brs: broad singlet.

The ligand **1** exhibited an orange color in toluene, while its lithium salt **2a** appeared reddish-purple (**Figure 1a**). The corresponding sodium salt **2b** exhibited bluish-purple hue whereas potassium **2c**, rubidium **2d**, and cesium **2e** salts exhibited purple colors. Notably, the color change from lithium salt **2a** to potassium salt **2c** is remarkable. To investigate this optical trend, the electronic absorption spectra for **1** and **2a**–**2e** were measured in toluene (**Figure 1b**). The ligand **1** displays an absorption maximum at 489 nm, while alkali metal salts **2a**–**2e** displayed absorption maxima around 570–590 nm with a large bathochromic shift of ca. 80–100 nm compared with that of ligand **1**. These red shifts suggest that the highest occupied molecular orbital (HOMO)– lowest unoccupied molecular orbital (LUMO)

energy gaps of alkali metal salts **2a**–**2e** were narrowed by coordination of alkali metals. However, the extent of the shift did not vary significantly among **2a**–**2e** (See; **Figure S2**).[4] Additionally, second absorption bands with weak intensity were observed around 400–450 nm in the spectra of **2a**–**2e**, which were absent in the spectrum of ligand **1**. The peak maxima of these bands differ depending on the alkali metal used, likely accounting for the color differences among the solution of **2a**–**2e** and relating to the electron density of the overall ligand framework (**Figure 2d)**.

Figure 1 (a) Solution colors. (b) electronic absorption spectra of **1** and **2a**–**2e** (1.0×10^{-4} M in toluene).

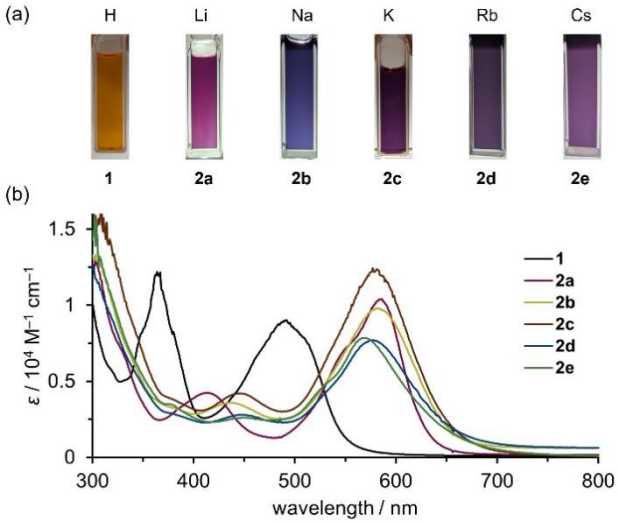

Figure 2 (a) Optimized structures. (b) selected energy diagrams of **2a**–**2e** calculated at the M06/def2TZVPP level of theory. (c) Ionic radii[5] and NPAs of M. *d* is the distance between alkali metals and mean plane of the phenalenyl scaffold of the ligand. (d) Electrostatic potentials for **2a**–**2e**.

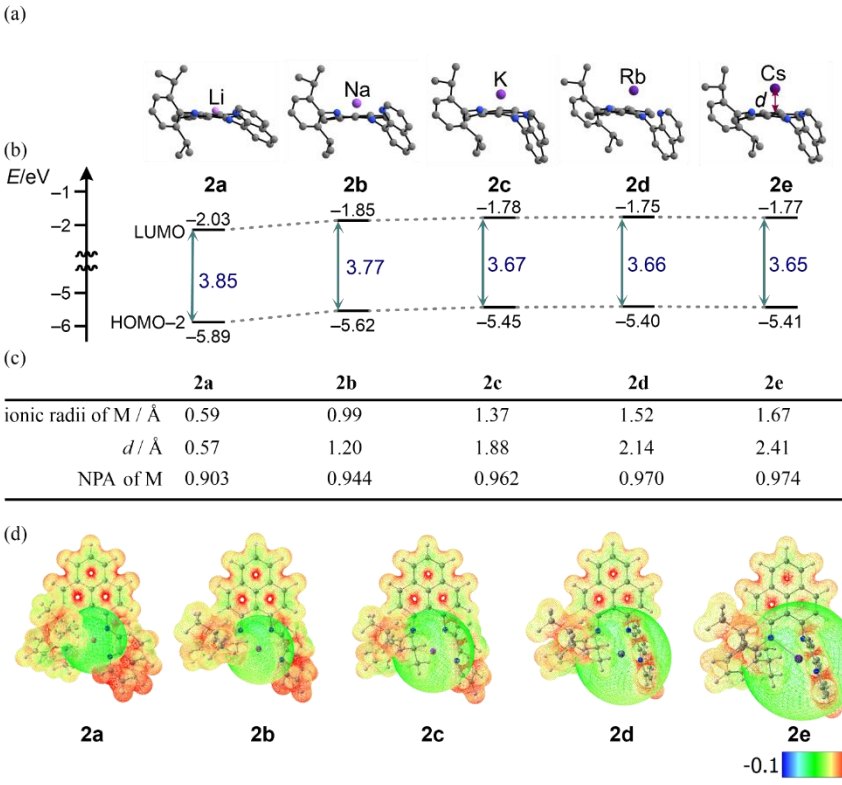

(c)

	2a	2b	2c	2d	2e
ionic radii of M / Å	0.59	0.99	1.37	1.52	1.67
d / Å	0.57	1.20	1.88	2.14	2.41
NPA of M	0.903	0.944	0.962	0.970	0.974

To gain further insights into the structures and electronic properties of **2a**–**2e**, density functional theory (DFT) calculations were performed at the M06[6]/def2TZVPP[7] level of theory (**Figure 2**). It was found that the distance *d*, from the mean plane of the phenalenyl scaffold of the ligand to the alkali metals increased with the ionic radius of the alkali metal. This trend could explain the broadening of the protons on the 2-position of quinoline moieties of heavier alkali metal salts (**Table 1**). DFT calculations also confirmed that alkali metal salts **2a**–**2e** possess narrower HOMO–LUMO gaps than that for **1**. Time dependent (TD)-DFT calculation predicted that the primary absorption bands observed in **2a**–**2e** around 570**–**590 nm were assignable to HOMO–LUMO transitions, which is consistent with the observed bathochromic shifts (**Figure 2b**). The secondary absorption bands for **2a**–**2e** were assignable to transitions from HOMO–2 to LUMO. The energy gap between HOMO–2 to LUMO decreased by ca. 0.1 eV from the lithium salt **2a** to the potassium salt **2b**, whereas only a slight decrease was observed among **2c**–**2e**. This observation is in agreement with the fact that a significant color change was noted among **2a**–**2c**, while the colors of **2c**–**2e** were similar. Natural population analyses (NPA)[8] revealed that heavier alkali metals possess a more positive charge, which correlates with the increased distance (*d*) between the alkali metals and the mean plane of the phenalenyl scaffold of the ligand (**Figure 2c**). Electrostatic potentials (ESPs) for **2a**–**2e** indicate that the ligands coordinated to lighter alkali metals exhibit more positive ESP charges compared to those coordinated to heavier alkali metals (**Figure 2d**). This trend aligns with the NPA results, where heavier alkali metals exhibit more positive natural charges. It should also be noted that the increase in HOMO–2 energy levels correlates with the natural charge of the metal.

1.3. Conclusion

In conclusion, this study elucidates the effect of alkali metal complexation on the electronic structure and optical properties of phenalenyl-based tridentate ligand **1**, providing a deeper insights into their structural and electronic nature, as well as potential applications in photofunctional propeties and reactivities.

1.4. Experimental Section

I. General Information.

^{1}H and ^{13}C NMR spectra were recorded on a JEOL ECS-400 spectrometer and JEOL ESZ-400S spectrometer. The chemical shifts were recorded relative to toluene (δ: 2.08 for 1H NMR in toluene-d_8) as an internal standard. Data are recorded as follows: chemical shifts in ppm (δ), multiplicity (s = singlet, d = doublet, t = triplet, sept = septet, brs = broad singlet, brd = broad doublet, m = multiplet), coupling constant (Hz), and integration. High resolution mass spectra (HRMS) were obtained using a JEOL JMS-T100LP spectrometer. Electronic absorption spectra were recorded on a JASCO V-770 spectrophotometer and an Agilent 8453 UV–vis spectroscopy system.

II. Materials.

All commercially available reagents and solvents were supplied from TCI, WAKO and Aldrich. The ligand **1** [3059559-13-3],[3] Rb-HMDS [143446-26-8][9] and Cs-HMDS [112549-87-8][10] were prepared according to literature procedure. All reactions with moisture- or air-sensitive compounds were performed in an argon-filled glove box.

III. Preparation of alkali metal salts 2a–2e.

Potassium salt K-DipQN-PLY (**2c**) was synthesized prepared by the reaction of ligand **1** with 1 equivalent of K-HMDS in THF. Other alkali salts M-DipQN-PLY (M = Li, Na, Rb, Cs; **2a**, **2b**, **2d**,and **2e**) were generated *in situ* by the reaction of ligand **1** with 1–2 equivalents of M-HMDS in toluene.

Synthesis of the ligand (1).[3]

A mixture of Me_3OBF_4 (11.1 g, 75.0 mmol) and **pre-1**[2] (17.8 g, 50.1 mmol) in DCE (500 mL) were stirred at rt for 15 h under a nitrogen atmosphere. ^{n}BuLi (1.6 M in hexane) (64 mL, 102 mmol) was added dropwise to 8-aminoquinoline (14.6 g, 101 mmol) at –78 °C in THF (150 mL). The reaction mixture was allowed to warm up to rt and stirred for 15 h and then, cooled to –78 °C. The lithium 8-quinolylamide solution was then added dropwise to the reaction mixture. The reaction mixture was allowed to warm up to room temperature and stirred for 4 h. The reaction mixture was quenched by adding water, MeOH, then the resulting solid was removed by filtration with MeOH. The solution was concentrated, and the resulting black slurry was extracted with $CHCl_3$. The organic layer was concentrated, and resulting black solid was washed with acetone to give the desired product **1** as a reddish-orange solid (6.78 g, 16.1 mmol, 32%)

Mp 235. 5–236.3 °C.

^{1}H NMR ($CDCl_3$, 400 MHz) δ: 14.93 (s, 1H), 8.76 (dd, J = 3.7, 1.8 Hz, 1H), 8.13 (dd, J = 8.5, 1.8 Hz, 1H), 7.78–7.69 (m, 4H), 7.60 (d, J = 9.2 Hz, 1H), 7.56–7.51 (m, 3H), 7.39–7.34 (m, 2H), 7.25–7.18 (m, 3H), 6.71 (d, J = 9.8 Hz, 1H), 3.19 (sep, J = 7.1 Hz, 2H), 1.14 (d, J = 7.1 Hz, 6H), 1.13 (d, J = 7.1 Hz, 6H).

^{13}C NMR ($CDCl_3$, 101 MHz) δ: 158.0, 153.5, 149.6, 142.8, 142.1, 142.0, 141.6, 135.9, 134.6, 133.9, 129.8, 129.6, 129.45, 129.40, 126.7, 126.6, 125.1, 123.3(two peaks were overlapped), 122.6, 121.9, 121.6, 119.4, 119.2, 118.8, 108.5, 28.6, 24.2, 23.2.

IR (KBr, cm^{-1}): 3056 w, 2962 m, 2918 w, 2861 w, 2630 s, 1601 m, 1589 s, 1520 m, 1442 m, 1412 m, 1382 m, 1321 m, 1181 w, 1371 m, 1057 w, 953 w, 839 m, 822 w, 810 m, 795 m, 779 m, 757 w, 657 w, 580 w.

HRMS (DART+) *m/z* $[M+H]^+$ Calcd for $C_{34}H_{32}N_3^+$: 482.2591, found: 482.2613.

Elemental Anal. Calcd. for $C_{34}H_{31}N_3$: C, 84.79; H, 6.49; N, 8.72. Found: C, 84.53; H, 6.45; N, 8.58.

Synthesis of K-DipQN-PLY (2c).

The ligand (0.49 g, 1.0 mmol) was dissolved in THF (6.3 mL) and K-HMDS (1.0M in THF) (2.5 mL, 2.5 mmol) was added to the solution. The color of the solution immediately changed from orange to dark purple. After stirring the reaction mixture for 3 h, the solvent was removed under reduced pressure and washed with hexane at least twice. The residue was dried in vacuo to obtain purple powder (0.47 g, 0.91 mmol, 90%).

1H NMR (toluene-*d*8, 400 MHz) δ: 7.99 (brs, 1H), 7.66 (d, J = 8.0 Hz, 1H), 7.44 (d, J = 7.5 Hz, 1H), 7.35 (d, J = 7.5 Hz, 1H), 7.30–7.22 (m, 3H), 7.16–7.07 (m, 3H, 1H was overlapped with solvent peak.), 7.06–6.99 (m, 3H), 6.96–6.91 (m, 1H), 6.77 (brs, 1H), 6.65 (d, J = 9.8 Hz, 1H), 3.28 (brs, 1H), 2.53 (brs, 1H), 1.14 (brs, 6H), 0.90 (brs, 6H).

^{13}C NMR measurement was unsuccessful because of the instability of **2c** in solution state.

HRMS (ESI+ in MeCN) m/z $[M+H]^+$ Calcd for $C_{34}H_{31}KN_3^+$:520.2150, found:520.2141.

General procedure for the preparation of M-DipQN-PLY) (2a, **2b**, **2d**, **2e).**

M-HMDS (M = Li, Na, Rb, Cs) (0.02 mmol for M = Na; 0.01 mmol for other metals) was added to a toluene-*d*8 (1.0 mL) solution of **1** (4.7 mg, 0.01 mmol) in a NMR tube equipped with J-Young valve in a glovebox at room temperature (1×10^{-2} M) and then, the change in the ^{1}H NMR chemical shifts were recorded. 0.1 mL of the solution above was diluted up to 2.0 mL with toluene (5×10^{-4} M) and transferred to 2 mm quartz cell equipped with ground glass stopper for electronic absorption spectra measurements.

Li-DipQN-PLY (**2a**)**.** ^{1}H NMR (toluene-d_8, 400 MHz) δ: 8.13 (brd, J = 9.2 Hz, 1H), 7.70 (brs, 2H), 7.54 (d, J = 8.8 Hz, 1H), 7.48 (d, J = 7.5 Hz, 1H), 7.40 (d, J = 8.8 Hz, 1H), 7.32 (d, J = 7.5 Hz, 1H), 7.28–7.18 (m, 6H), 6.89-6.77 (m, 5H), 6.74 (brd, J = 7.5 Hz, 2H), 6.66 (dd, J = 16.4 Hz, 7.8 Hz, 1H), 3.29 (sept, J = 6.9 Hz, 2H), 1.12 (d, J = 6.9 Hz, 7H), 1.03 (d, J = 6.9 Hz, 6H).

^{13}C NMR and HRMS measurement were unsuccessful because of the instability of **2a** in solution state.

Na-DipQN-PLY (**2b**)**.** ^{1}H NMR (toluene-d_8, 400 MHz) δ: 7.70 (d, J = 9.2 Hz, 1H), 7.64 (d, J = 8.0 Hz, 1H), 7.60 (brs, 1H), 7.47 (d, J = 7.5 Hz, 1H), 7.39 (d, J = 8.0 Hz, 1H), 7.37–7.30 (m, 2H), 7.26–7.21 (m, 1H), 7.21–7.17 (m, 2H), 7.07–7.00 (m, 3H), 6.96–6.91 (m, 1H), 6.78-6.70 (m, 2H), 3.22 (brs, 2H), 1.16 (brd, J = 6.3 Hz, 6H), 1.00 (brd, J = 6.3 Hz, 6H).

^{13}C NMR and HRMS measurement were unsuccessful because of the instability of **2b** in solution state.

Rb-DipQN-PLY (**2d**)**.** ^{1}H NMR (toluene-d_8, 400 MHz) δ: 7.94 (brs, 1H), 7.65 (d, J = 8.0 Hz, 1H), 7.44 (d, J = 7.5 Hz, 1H), 7.37 (d, J = 7.5 Hz, 1H), 7.28 (t, J = 7.8 Hz, 1H), 7.23–7.16 (m, 3H), 7.14–7.10 (m, 3H), 7.07–6.99 (m, 4H), 6.92 (brd, J = 7.5 Hz, 1H), 6.75 (q, J = 8.0 Hz, 4.0 Hz, 1H), 6.65 (d, J = 9.8 Hz, 1H), 3.30 (brs, 1H), 2.50 (brs, 1H), 1.12 (d, J = 6.3 Hz, 6H), 0.85 (brs, 6H).

^{13}C NMR and HRMS measurement were unsuccessful because of the instability of **2d** in solution state.

Cs-DipQN-PLY (**2e**)**.** ^{1}H NMR (toluene-d_8, 400 MHz) δ: 7.98 (brs, 1H), 7.65 (s, 1H), 7.44–7.28 (m, 4H), 7.18–7.11 (m, 3H), 7.07–6.99 (m, 5H), 6.79 (brs, 1H), 6.72–6.63 (m, 1H), 3.35 (brs, 1H), 2.59 (brs, 1H), 1.19 (brs, 6H), 0.89 (brs, 6H).

^{13}C NMR and HRMS measurement were unsuccessful because of the instability of **2e** in solution state.

IV. Electronic Absorption Spectra.

0.1 mL of the toluene-d_8 solution of **1** and **2a**–**2e** prepared above were diluted up to 2.0 mL with toluene (5×10^{-4} M) and transferred to 2 mm quartz cell equipped with ground glass stopper in a glove box. Electronic absorption spectra measurements for **1** and **2a**–**2e** were recorded in toluene at 25 °C.

V. Computational Details.

All calculations were conducted using the Gaussian 16 (G16 Rev C.01).[11] Optimization was performed at the M06/def2TZVPP level of theory. Harmonic vibration frequency analysis was conducted with the optimized structures at the same level of theory to verify all stationary points as local minima (with no imaginary frequency). Each reported minimum has no imaginary frequency. All structures, orbitals and spin density maps were visualized by GaussView 6.1.1[12] and Chemcraft Version 1.8. [13]

Figure S1 (a) Optimized structures. (b) selected energy diagrams of **2a**–**2e** calculated at the M06/def2TZVPP level of theory. (c) Ionic radii and NPAs of M. *d* are the distances between alkali metals mean plane of phenalenyl scaffold of the ligand.

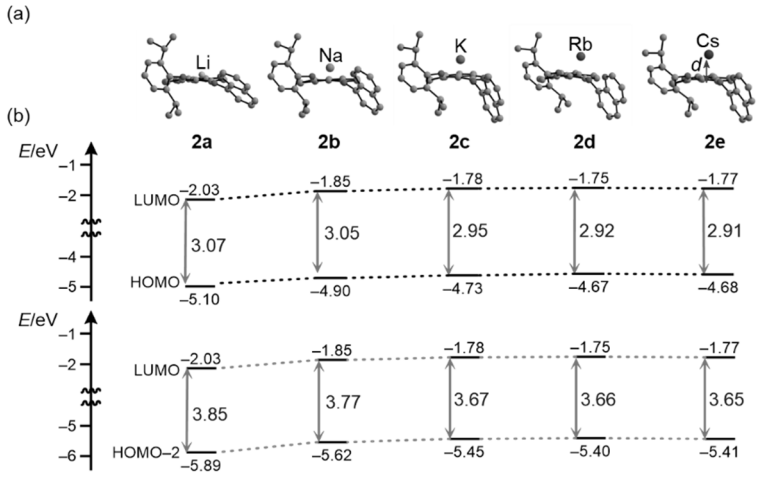

(c)

	2a	2b	2c	2d	2e
ionic radii of M / Å	0.59	0.99	1.37	1.52	1.67
d / Å	0.57	1.20	1.88	2.14	2.41
NPA of M	0.903	0.944	0.962	0.970	0.974

Figure S2. Selected molecular orbitals of **2a**–**2e** calculated at the M06/def2TZVPP level of theory.

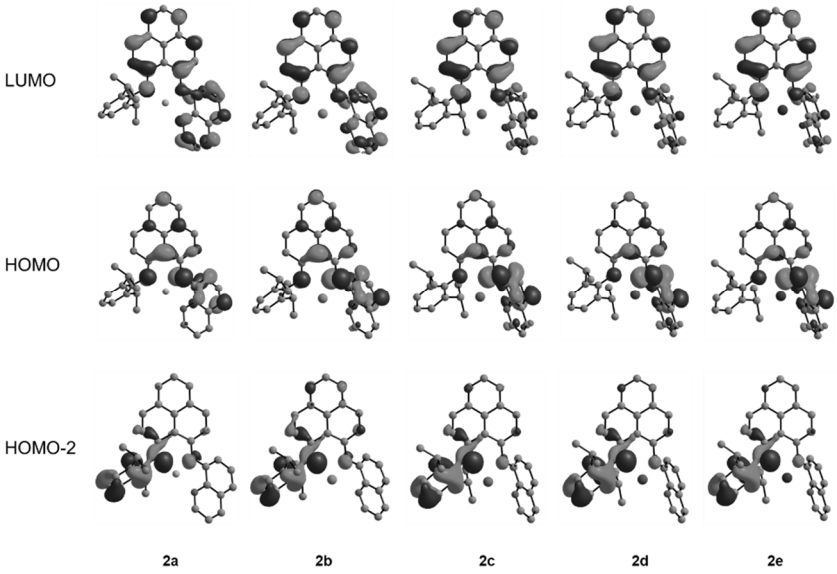

VI. Cartesian Coordinates and Energies of Optimized Structures.

1

H	-0.47965600	-0.04717100	0.04161100	H	-5.81374800	0.57919600	-1.37751900
N	0.08559900	-0.90083400	0.15642900	C	1.12451800	1.80138900	-0.08481300
N	-2.54566000	0.76000100	-0.65588400	C	0.77130400	-3.70169700	-3.03773100
N	-0.16210000	1.67430000	0.06282500	H	-0.03760100	-4.27240200	-3.49978700
C	-4.88164100	1.04066300	-1.07975100	H	1.37878500	-4.39186000	-2.44924000

H	1.38990400	-3.31300300	-3.84795100	C	5.35509800	2.14625600	-0.10346600
C	-4.80997900	2.36572800	-0.76637300	H	5.79188000	3.11517800	-0.31882900
H	-5.68929400	2.99940000	-0.80315300	C	-1.97975800	-4.52827600	0.16998500
C	3.97465000	2.02062700	-0.13274000	H	-2.51983100	-5.46695000	0.17704000
C	2.27944600	-1.77373700	0.53161300	C	4.21515700	-0.33847900	0.39411900
H	1.83913200	-2.75235400	0.67870400	C	-2.23083000	4.74449500	0.42010600
C	3.13421600	3.12197800	-0.47888900	H	-2.12948600	5.77216800	0.74697600
H	3.60983400	4.05469000	-0.76409400	C	5.60273600	-0.16581700	0.42758800
C	-1.39842900	-2.45647200	1.25470500	H	6.22506200	-1.02746800	0.64223800
C	-3.70879200	0.27112900	-0.99644400	C	-1.10010700	3.91649000	0.43420500
H	-3.74192200	-0.79415400	-1.21957100	H	-0.16577000	4.31086900	0.81043500
C	-0.58212900	-2.14959700	0.16097400	C	0.24297700	-2.55399700	-2.19522300
C	-0.66947900	-1.65543700	-3.02593400	H	1.10396700	-1.95507100	-1.88976800
H	-0.15167200	-1.29554300	-3.91734100	C	-1.19916100	-4.19060000	-0.92014700
H	-1.01155600	-0.79048800	-2.45326300	H	-1.14842100	-4.86505300	-1.76551100
H	-1.55092500	-2.21615200	-3.35079600	C	6.17376300	1.06266300	0.18635100
C	3.61982600	-1.60425800	0.60621200	H	7.24870000	1.18232800	0.21063700
H	4.26240200	-2.45089100	0.82111400	C	-3.44594200	4.27902600	0.00631200
C	-2.08670500	-3.66293700	1.24144200	H	-4.31700000	4.92308000	-0.01280400
H	-2.71659000	-3.92956700	2.08103700	C	-1.48974600	-1.51210400	2.42976600
C	-1.16461200	2.59535700	0.02637700	H	-1.32136100	-0.49897600	2.05293000
C	1.79352900	3.02217300	-0.47001100	C	-0.38597400	-1.82407000	3.43410100
H	1.18260300	3.86468000	-0.76269400	H	-0.50548800	-2.83935500	3.82274600
C	-0.49593200	-2.99359700	-0.95311200	H	-0.42026200	-1.13269900	4.27837900
C	-2.45235300	2.07392800	-0.35302500	H	0.60354100	-1.75346600	2.97871500
C	1.95647800	0.62307500	0.11426600	C	-2.84800700	-1.52100700	3.10977000
C	-3.58026300	2.92901100	-0.37627500	H	-3.65487100	-1.35132200	2.39468000
C	3.36660600	0.76578100	0.13292800	H	-2.89153900	-0.73261400	3.86277500
C	1.40420900	-0.68001800	0.27056400	H	-3.04174200	-2.46532200	3.62404500

Method: M06/def2TZVPP opt freq

imaginary frequencies: 0

EE + Thermal Free Energy Correction: − 1477.489810 Hartree

2a

Li	-1.12281700	-0.69095400	-0.70424000	C	0.59297300	4.23194400	-0.62656100
N	0.67279100	-0.87155300	-0.08064100	H	0.41525200	5.25497800	-0.94073300
N	-3.12216500	-0.66464900	-0.99197900	C	0.50873700	-2.89748100	1.23339800
N	-1.26676800	1.11976900	-0.20992800	C	-3.99804600	-1.55176900	-1.39966500
C	-5.38242100	-1.35728400	-1.32527000	H	-3.60413900	-2.47861000	-1.80684100
H	-6.05645800	-2.12097100	-1.68815800	C	1.04261600	-2.21396700	0.12597900
C	-0.23154300	1.96245700	-0.24894800	C	1.46530700	-2.54745800	-3.25346700
C	3.80205200	-2.50040700	-2.35026100	H	1.79360300	-2.01714700	-4.14976700
H	3.95521400	-3.54894200	-2.61525800	H	0.41999400	-2.28695500	-3.07032500
H	4.43348900	-2.27606600	-1.48877900	H	1.50657400	-3.61987700	-3.46104200
H	4.15166200	-1.90011300	-3.19218900	C	3.73602700	0.81105200	0.84287900
C	-5.84332500	-0.19973400	-0.76980800	H	4.72908900	0.56404900	1.20346800
H	-6.90694800	-0.01333800	-0.67074800	C	0.80091300	-4.24540400	1.39070600
C	1.90052200	3.86060400	-0.23022300	H	0.40764300	-4.77875400	2.24803600
C	2.79942100	-0.14417200	0.72958500	C	-2.57185600	1.47031800	-0.03235200
H	3.03444200	-1.16941100	0.98729000	C	-0.41541200	3.33812400	-0.61555800

H	-1.40331100	3.64142700	-0.93342700	C	2.34125200	-2.19711400	-2.05630700
C	1.82944200	-2.89507900	-0.81759900	H	2.25936100	-1.12073800	-1.89509800
C	-3.55693700	0.50753900	-0.46118800	C	2.08339200	-4.24604300	-0.62306700
C	1.11061800	1.51827000	0.00315600	H	2.68543300	-4.78209700	-1.34811300
C	-4.94022300	0.77174500	-0.30143100	C	4.20079400	4.45093200	0.22694400
C	2.14445300	2.49830800	0.08091200	H	4.98679100	5.19233800	0.28029300
C	1.47383500	0.12316400	0.21564200	C	-5.36300700	1.95795700	0.32646700
C	2.92771000	4.80335800	-0.16462400	H	-6.42231900	2.14791900	0.44555500
H	2.69877700	5.83059300	-0.42614300	C	-0.32271700	-2.16154200	2.25942600
C	1.58367100	-4.92106800	0.47387500	H	-0.78124100	-1.30074600	1.75991100
H	1.79908400	-5.97310500	0.61140200	C	0.56818600	-1.61063100	3.36765600
C	3.46327200	2.16117000	0.48537300	H	1.07641500	-2.43054700	3.88303500
C	-4.42120500	2.82781700	0.80090600	H	-0.02043500	-1.06060300	4.10483900
H	-4.73213500	3.72474700	1.32295400	H	1.33198900	-0.93770400	2.97410600
C	4.45505400	3.13054700	0.55798600	C	-1.44173500	-3.00186100	2.85304800
H	5.44488700	2.83031400	0.88377600	H	-2.05957400	-3.46053100	2.07865000
C	-3.05376400	2.59281200	0.63137400	H	-2.08555600	-2.37998800	3.47728100
H	-2.34892000	3.29636600	1.05301700	H	-1.05555700	-3.80123100	3.48968300

Method: M06/def2TZVPP opt freq

imaginary frequencies: 0

EE + Thermal Free Energy Correction: − 1484.505990 Hartree

2b

Na	-0.99233000	-1.22860200	-1.16443700	H	4.67665700	1.33021500	1.30535100
N	0.94596200	-0.81051700	-0.06786500	C	1.31494100	-4.14564300	1.46378800
N	-3.31623900	-0.85194300	-1.32225000	H	0.88136700	-4.72908700	2.28227000
N	-1.35587500	0.83065800	-0.26368500	C	-2.66193600	1.03760800	0.05854300
C	-5.61443600	-1.49701100	-1.58903400	C	-0.86413300	3.15472200	-0.65084700
H	-6.33264100	-2.17279000	-2.05933200	H	-1.90855400	3.28861600	-0.94501900
C	-0.44749000	1.81824800	-0.28537700	C	2.43857800	-2.67429000	-0.64146300
C	4.51071100	-2.04280000	-1.95986000	C	-3.68186100	0.15677500	-0.48494400
H	4.82896400	-3.07465200	-2.18808000	C	0.95829700	1.61925200	-0.02269300
H	5.01604500	-1.73368100	-1.03028100	C	-5.05581500	0.35271300	-0.13249200
H	4.88359400	-1.40276900	-2.77645200	C	1.81496000	2.76901100	0.04222100
C	-6.01129300	-0.50707300	-0.72521700	C	1.55453700	0.30949600	0.23885800
H	-7.06845100	-0.36639000	-0.47521700	C	2.20735800	5.17994800	-0.26048900
C	1.34691100	4.07160500	-0.30203400	H	1.80673200	6.15756400	-0.55027800
C	2.88820500	0.28416900	0.81881200	C	2.28054700	-4.72876900	0.64909800
H	3.28063700	-0.68875600	1.13169500	H	2.60232500	-5.75901800	0.82647900
C	-0.01675500	4.21296100	-0.68755100	C	3.17195200	2.66915000	0.47874500
H	-0.37355400	5.19774100	-1.00964700	C	-4.44633700	2.15273300	1.33813300
C	0.88702700	-2.83318400	1.25538400	H	-4.71358400	2.92108700	2.07054200
C	-4.23621900	-1.63558600	-1.84482400	C	3.99414800	3.79823300	0.52712800
H	-3.89016200	-2.43858100	-2.51052500	H	5.02452700	3.67526200	0.87853400
C	1.46824700	-2.08019000	0.20138600	C	-3.09868400	1.99321300	0.98994700
C	2.30650800	-2.37885000	-3.11576800	H	-2.34703500	2.62578500	1.47098100
H	2.66461600	-1.81174700	-3.99138000	C	2.99791300	-1.92381500	-1.83319900
H	1.21138400	-2.24386500	-3.05766500	H	2.76582500	-0.85411300	-1.69687000
H	2.49230400	-3.45043600	-3.30687400	C	2.82667400	-3.99405300	-0.39705700
C	3.65751000	1.39244200	0.90686100	H	3.57506200	-4.46045700	-1.04753500

C	3.52697300	5.05419900	0.14703300	H	1.14438500	-2.06631700	3.90415100
H	4.18535800	5.92607500	0.18188300	H	-0.20531100	-0.89746100	3.91773900
C	-5.42921400	1.36456300	0.78007500	H	1.20817200	-0.61482800	2.87268400
H	-6.48500100	1.49151000	1.03690800	C	-1.14576400	-3.16830300	2.74973200
C	-0.14397300	-2.18710100	2.15924800	H	-1.61198700	-3.80340000	1.97778900
H	-0.70270700	-1.45238100	1.54553400	H	-1.94969200	-2.62510200	3.27238600
C	0.53827000	-1.39334600	3.27151400	H	-0.67871700	-3.83695800	3.49370700

Method: M06/def2TZVPP opt freq

imaginary frequencies: 0

EE + Thermal Free Energy Correction: − 1477.489810 Hartree

2c

K	-0.93443800	-1.12226800	-2.02139300	C	-3.45218800	0.79337500	-0.46590900
N	0.89218000	-0.89641400	-0.13790800	C	1.35234500	1.47128200	-0.13374700
N	-3.39170700	-0.12290600	-1.46587500	C	-4.69931800	1.11288400	0.16385000
N	-1.03860300	1.08833500	-0.55776600	C	2.39713000	2.44330400	-0.01955500
C	-5.76637500	-0.46432300	-1.32996000	C	1.65054500	0.09133800	0.25073300
H	-6.64544800	-0.98908300	-1.71225000	C	3.26089300	4.71626200	-0.36400700
C	0.03237500	1.90494400	-0.49414600	H	3.08090600	5.73952400	-0.71158600
C	4.41954400	-3.11505700	-0.74968500	C	0.89900300	-4.89508500	1.13243700
H	4.53632500	-4.21250700	-0.75265100	H	0.87257300	-5.94030300	1.45403900
H	4.67639600	-2.75540400	0.25979800	C	3.65694300	2.11021300	0.56520900
H	5.16513400	-2.70846700	-1.45297300	C	-3.58827700	2.63868700	1.65086800
C	-5.85693700	0.44972900	-0.31004200	H	-3.61092600	3.34637100	2.48606200
H	-6.82053800	0.68077100	0.15708100	C	4.67691800	3.06105100	0.63726100
C	2.20332000	3.79311600	-0.43229500	H	5.62719700	2.77311000	1.10033700
C	2.84408100	-0.13058000	1.05297800	C	-2.35842400	2.34853900	1.04908800
H	2.97440400	-1.12074100	1.50211900	H	-1.44957300	2.81074200	1.44649900
C	0.90377100	4.17802000	-0.87179100	C	3.01230000	-2.69223700	-1.15206100
H	0.74629200	5.20912200	-1.20788100	H	3.00130800	-1.58984500	-1.19965400
C	-0.05753600	-2.66236800	1.17973000	C	1.89284200	-4.45341600	0.26793000
C	-4.49204200	-0.71879800	-1.87423500	H	2.64323600	-5.16485600	-0.09573900
H	-4.39280600	-1.45478400	-2.68613600	C	4.49626900	4.35677700	0.15212100
C	0.98407100	-2.20971800	0.32267700	H	5.30909300	5.08583800	0.20632900
C	2.67405100	-3.21263800	-2.54665900	C	-4.75791600	2.04643000	1.22247400
H	3.40874400	-2.87025300	-3.29487900	H	-5.72208900	2.26955500	1.68878600
H	1.67694900	-2.87204500	-2.87793400	C	-1.10178900	-1.67335300	1.65833300
H	2.66162400	-4.31647800	-2.56712600	H	-1.24334500	-0.93838900	0.84433700
C	3.81325400	0.80821100	1.14953700	C	-0.59113600	-0.87253500	2.85413200
H	4.74307000	0.59228500	1.68865800	H	-0.38551000	-1.53944400	3.71110600
C	-0.07033000	-3.99886000	1.57800400	H	-1.33995900	-0.12694800	3.17266900
H	-0.86019900	-4.35164400	2.24922300	H	0.33992600	-0.33038800	2.61926300
C	-2.22958400	1.44924800	-0.02756200	C	-2.45534200	-2.29222400	1.97060000
C	-0.12955800	3.29535000	-0.84994900	H	-2.82781500	-2.91905000	1.14163700
H	-1.12987100	3.61180000	-1.16068900	H	-3.19834600	-1.49618400	2.15056700
C	1.95623300	-3.12111900	-0.15306200	H	-2.43032000	-2.92100400	2.87850800

Method: M06/def2TZVPP opt freq

imaginary frequencies: 0

EE + Thermal Free Energy Correction: − 2076.862647 Hartree

2d

Rb	-0.87283300	-1.07257400	-2.09886200	C	-3.37398300	0.97658900	-0.27067900
N	0.90593600	-0.85813400	0.03356600	C	1.45154300	1.49029500	-0.05356500
N	-3.37155300	0.04876300	-1.26028500	C	-4.58993600	1.33882400	0.39582300
N	-0.95682600	1.18751500	-0.43213200	C	2.53536600	2.42352000	0.01063300
C	-5.74614500	-0.23876500	-1.02965300	C	1.69941000	0.11498000	0.38391900
H	-6.65011300	-0.75024900	-1.36967600	C	3.48473600	4.64399200	-0.43537300
C	0.14456500	1.96307200	-0.41155300	H	3.34153800	5.65901700	-0.82204600
C	4.39411500	-3.18473500	-0.44095200	C	0.79380400	-4.81415200	1.42879700
H	4.48272800	-4.28424000	-0.40599100	H	0.73738500	-5.84676800	1.78543000
H	4.64315400	-2.79888900	0.56067500	C	3.78659100	2.06466700	0.59906800
H	5.16189200	-2.82043300	-1.14362300	C	-3.38932700	2.86394500	1.81277300
C	-5.77869200	0.69416300	-0.02341500	H	-3.36571700	3.58943300	2.63258300
H	-6.71912300	0.95476800	0.47446000	C	4.84461900	2.97537200	0.62056900
C	2.38990600	3.76275300	-0.45344900	H	5.78708600	2.66981700	1.08832800
C	2.88476900	-0.11509900	1.19693700	C	-2.18802800	2.52805200	1.17811700
H	2.97490000	-1.08569400	1.69567400	H	-1.25425800	2.97233800	1.53676600
C	1.09949700	4.18421300	-0.88643000	C	3.00515900	-2.74086300	-0.88284000
H	0.97767800	5.20847900	-1.25655600	H	3.02534100	-1.64097100	-0.96998800
C	-0.11514300	-2.56172600	1.37593200	C	1.81635000	-4.42350300	0.57350000
C	-4.49878500	-0.52783200	-1.61860800	H	2.55846200	-5.16322900	0.25169700
H	-4.44702400	-1.27624100	-2.42449600	C	4.71081100	4.25575000	0.08171800
C	0.95772600	-2.15925200	0.53212700	H	5.55295300	4.95271500	0.09704900
C	2.68037200	-3.30286500	-2.26479900	C	-4.58789100	2.29310700	1.43746700
H	3.43471000	-3.00118400	-3.01126700	H	-5.52909400	2.54942500	1.93281600
H	1.69544300	-2.95603400	-2.62400400	C	-1.15490200	-1.53796100	1.78418600
H	2.64652600	-4.40630500	-2.24737400	H	-1.27683700	-0.85074200	0.92634300
C	3.89226400	0.78619400	1.24487400	C	-0.65654100	-0.67188300	2.93914400
H	4.81444000	0.55908900	1.79258100	H	-0.48043800	-1.28633000	3.84071900
C	-0.16633300	-3.88271000	1.81912800	H	-1.40096900	0.10361000	3.19054500
H	-0.98036200	-4.19583400	2.48088000	H	0.28699500	-0.15782300	2.69163700
C	-2.11902600	1.60049100	0.11958000	C	-2.51702300	-2.12700000	2.11568400
C	0.03143500	3.34649900	-0.81284000	H	-2.89088400	-2.79140900	1.31731000
H	-0.96234200	3.69317900	-1.11291000	H	-3.25347600	-1.31630200	2.25291400
C	1.91958500	-3.10744500	0.10999100	H	-2.50387200	-2.70908200	3.05450900

Method: M06/def2TZVPP opt freq

imaginary frequencies: 0

EE + Thermal Free Energy Correction: − 1501.018338 Hartree

2e

Cs	-0.82207600	-1.05446200	-2.13522800	C	4.16110100	-3.31413000	-0.10012500
N	0.85908700	-0.82107700	0.24281300	H	4.21768900	-4.39844600	0.09792200
N	-3.31152400	0.31662300	-1.09411100	H	4.40722800	-2.79053900	0.83744300
N	-0.82125800	1.32637100	-0.35226500	H	4.94683000	-3.07447000	-0.83600300
C	-5.68258900	0.12328800	-0.76215000	C	-5.63815300	1.07444500	0.22688300
H	-6.61866200	-0.35920100	-1.05452500	H	-6.54687100	1.37977700	0.75725400
C	0.33391300	2.01890900	-0.36121500	C	2.71418000	3.62953200	-0.49761500

C	2.90930900	-0.18917900	1.34371300	C	0.44705600	-4.69383100	1.79958400
H	2.92333800	-1.13631900	1.89291100	H	0.31653200	-5.70153100	2.20479500
C	1.45590500	4.13491200	-0.93577200	C	3.98126000	1.87439000	0.62514000
H	1.41162100	5.14953900	-1.34756500	C	-3.09113600	3.18734400	1.91495500
C	-0.28978200	-2.38394300	1.64715000	H	-3.00593400	3.93221100	2.71312200
C	-4.47287700	-0.22008600	-1.39880200	C	5.11003200	2.69463400	0.59264200
H	-4.48090400	-0.98030900	-2.19615100	H	6.03012100	2.33626400	1.06738600
C	0.80920500	-2.10055600	0.78839800	C	-1.92941800	2.78397600	1.24668600
C	2.48202900	-3.63378000	-1.93165100	H	-0.96454500	3.19331900	1.56209000
H	3.25101400	-3.42381900	-2.69444900	C	2.78674300	-2.91044700	-0.62181200
H	1.50330000	-3.33563400	-2.34831400	H	2.82253100	-1.82874700	-0.84104800
H	2.44673900	-4.72742100	-1.78642100	C	1.48543500	-4.42260700	0.91805600
C	3.98904800	0.62517700	1.33488600	H	2.16468200	-5.23101600	0.62274500
H	4.89637200	0.35028000	1.88572000	C	5.07442000	3.95443600	-0.00775800
C	-0.43791600	-3.67527900	2.15001800	H	5.97096700	4.57950700	-0.03398000
H	-1.27058100	-3.89553600	2.82610400	C	-4.32633900	2.65676200	1.60342200
C	-1.94014800	1.82304400	0.21541200	H	-5.23514200	2.96361600	2.12962100
C	0.32463900	3.38926300	-0.81682300	C	-1.25228800	-1.26797200	1.99581400
H	-0.64272300	3.80062900	-1.12181200	H	-1.30927500	-0.61747400	1.10382700
C	1.68444300	-3.14052400	0.39378300	C	-0.70440300	-0.39088500	3.11914700
C	-3.23690100	1.25568300	-0.11980500	H	-0.58083100	-0.97691900	4.04807100
C	1.60113600	1.46215200	0.01612800	H	-1.39414000	0.44538200	3.32893000
C	-4.40951300	1.68069200	0.58532300	H	0.27581300	0.04400300	2.86163800
C	2.75699400	2.30585800	0.02851800	C	-2.66110600	-1.73501100	2.32635000
C	1.73728500	0.09655800	0.52963600	H	-3.06216700	-2.42321200	1.56208200
C	3.87787400	4.41775900	-0.53168400	H	-3.33856700	-0.86489100	2.38627500
H	3.81315900	5.42195400	-0.96490100	H	-2.71419500	-2.25251800	3.30115300

Method: M06/def2TZVPP opt freq

imaginary frequencies: 0

EE + Thermal Free Energy Correction: − 1497.081388 Hartree

1.5. References

1. (a) Tsai, Y.-C. *Coord. Chem. Rev.* **2012**, *256*, 722. (b) Camp, C.; Arnold, J. *Dalton Trans.* **2016**, *45*, 14462.

2. (a) Kodama, T.; Mukai, N.; Tobisu, M. *Inorg. Chem*. **2023**, *62*, 6554. (b) Kodama, T.; Uchida, K.; Nakasuji, C.; Kishi, R.; Kitagawa, Y.; Tobisu, M. *Inorg. Chem*. **2023**, *62*, 7861.

3. Noguchi, H.; Kodama, T.; Kikkawa, S.; Yamazoe, S.; Tobisu, M. *Chem. Lett.* **2024**, *53*, upae236.

4. HOMOs of 2a–2e are distributed among the π-orbitals of the phenalenyl scaffold, whereas the corresponding LUMOs reside in the π*-orbitals of the phenalenyl. The HOMO–2 orbitals are mainly distributed over the π-orbitals of the diisopropylphenylamino groups (**Figure S2**).

5. Shannon, R. D. *Acta Cryst. A* **1976**, *32*, 751.

6. Zhao, Y.; Truhlar, D. G.; *Theor. Chem. Acc.* **2008**, *120*, 215.

7. (a) Weigend, F.; Ahlrichs, R. *Phys. Chem. Chem. Phys*. **2005**, *7*, 3297. (b) Weigend, F. *Phys. Chem. Chem. Phys*. **2006**, *8*, 1057. (c) Zheng, J.; Xu, X.; Truhlar, D. G. *Theor. Chem. Acc.* **2011**, *128*, 295.

8. Reed, A. E.; Weinstock, R. B.; Weinhold, F. *J. Chem. Phys*. **1985**, *83*, 735

9. Evans, M. J.; Jones, C. *Inorg. Chem*. **2023**, *62*, 14393.

10. Ojeda-Amador, A. I.; Martínez-Martínez, A. J.; Kennedy, A. R.; O'Hara, C. T. *Inorg. Chem*. **2016**, *55*, 5719.

11. Frisch, M. J.; Trucks, G. W.; Schlegel, H. B.; Scuseria, G. E.; Robb, M. A.; Cheeseman, J. R.: Scalmani, G.; Barone, V.; Mennucci, B.; Petersson, G. A.; Nakatsuji, H.; Caricato, M.; Li, X.; Hratchian, H. P.; Izmaylov, A. F.; Bloino, J.; Zheng, G.; Sonnenberg, J. L.; Hada, M.; Ehara, M.; Toyota, K.; Fukuda, R.; Hasegawa, J.; Ishida, M.; Nakajima, T.; Honda, Y.; Kitao, O.; Nakai, H.; Vreven, T.; Montgomery, Jr., J. A.; Peralta, J. E.; Ogliaro, F.; Bearpark, M.; Heyd, J. J.; Brothers, E.; Kudin, K. N.; Staroverov, V. N.; Keith, T.; Kobayashi, R.; Normand, J.; Raghavachari, K.; Rendell, A.; Burant, J. C.; Iyengar, S. S.; Tomasi, J.; Cossi, M.; Rega, N.; Millam, J. M.; Klene, M.; Knox, J. E.; Cross, J. B.; Bakken, V.; Adamo, C.; Jaramillo, J.; Gomperts, R.; Stratmann, R. E.; Yazyev, O.; Austin, A. J.; Cammi, R.; Pomelli, C.; Ochterski, J. W.; Martin, R. L.; Morokuma, K.; Zakrzewski, V. G.; Voth, G. A.; Salvador, P.; Dannenberg, J. J.; Dapprich, S.; Daniels, A. D.; Farkas, O.; Foresman, J. B.; Ortiz, J. V.; Cioslowski, J.; Fox, D. J. Gaussian, Inc., Wallingford CT, **2016**.
12. Dennington, R.; Keith, T. A.; Millam, J. M.; Semichem Inc., Shawnee Mission, KS, **2016**.
13. G. A. Andirenko, https://www.chemcraftprog.com.

Chapter 2

A nickel metalloradical bearing a phenalenyl-based tridentate ligand

2.1. Introduction

Nickel(I) complexes play pivotal roles in various chemical[1] and biological[2] transformations. However, the exploration of discrete Ni(I) complexes has been somewhat limited compared with that of Ni(0) and Ni(II) complexes due to their inherent instabilities and paramagnetic nature. The electronic configuration of Ni(I) complexes is heavily influenced by the surrounding geometry, which is modulated by the ligand environment.[3] Among these, Ni(I) complexes adopting a T-shaped geometry have garnered significant interest owing to their distinctive properties and reactivities that stem from the unpaired electron accommodated in the energetically destabilized and geometrically exposed $d_{x^2-y^2}$ orbital.[4] In 2005, Holland first reported a crystalline Ni(I) complex bearing β-diketiminate and a monodentate ligand (CO) accommodating a T-shaped geometry, rather than the sterically favored Y-shaped geometry (**Figure 1A**).[5] Since the pioneering work by Caulton in 2008(Fig. Figure 1B),[6] several isolable tridentate T-shaped Ni(I) complexes have been reported (**Figure 1C to H**).[7]

Noteworthy among these is a systematic investigation by Lee et al. into the reactivity of a T-shaped Ni(I) complex featuring a rigid acridane-based tridentate ligand (**Figure 1D**),[7b] which behaves as a metalloradical, in reaction such as the homolysis of a carbon–halogen bond and addition to ethylene or CO2. These studies underscore the potential utility of T-shaped Ni(I) complexes as novel platforms for radical reagents and/or catalysts. Consequently, the development of new ligands tailored for T-shaped Ni(I) complexes has emerged as a critical pursuit within the realm of organometallic chemistry.

Figure 1 Representative examples of T-shaped Ni(I) complexes. Dip, 2,6-diisopropylphenyl.

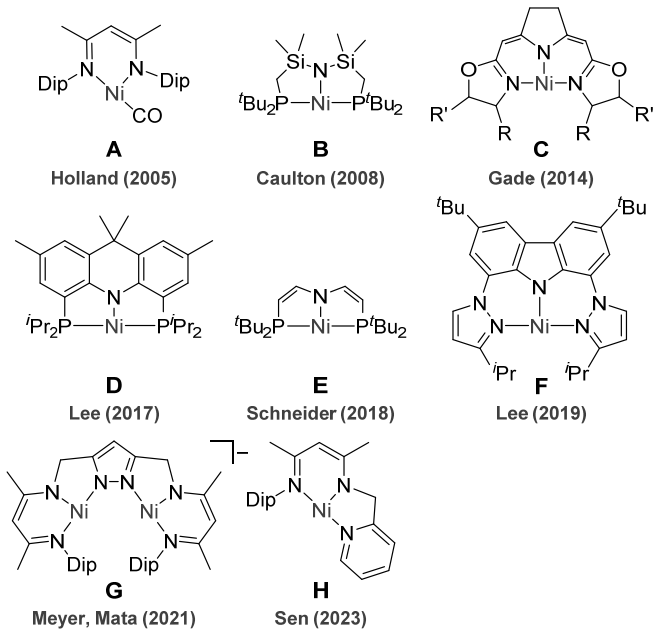

2.2. Results and Discussion

Recently, our group reported low-valent, main-group element complexes that bear a phenalenyl-based bidentate ligand (DipN-PLY).[8] Furthermore, N,N,N-tridentate PLY ligand (DipQN-PLY) was also reported with alkali metal salts for further transmetallation to transition metal complexes.[9] We envisioned the tridentate ligand could serve as a new tridentate ligand for a Ni(I) complex. Herein, we detail the synthesis, properties, and reactivity of the Ni(I) complex **1** (**Scheme 1**) that facilitates metalloradical reactivity.

Scheme 1 Synthetic scheme of alkali metal salts.

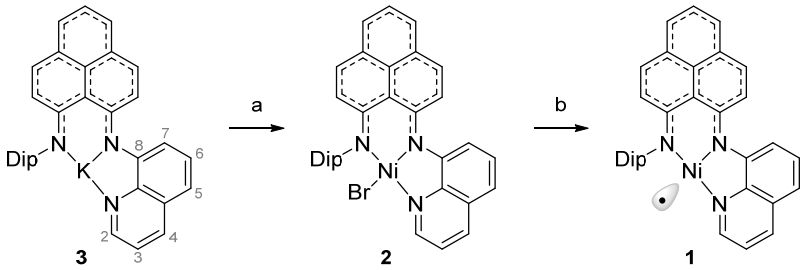

Reaction conditions; (a) KHMDS (1 M in THF, 1.2 equiv), THF, −35 °C to rt, 3 h, and then $NiBr_2$(dme) (1.2 equiv), −35 °C to 65 °C, 15 h, 86%. (b) KH (3.5 equiv), THF, rt, 15 h. dme = 1,2-dimethoxyethane.

Nickel(II) bromide precursor **2** was obtained as a mixture of diastereomers by reacting K-DipQN-PLY[9] **3** with $NiBr_2$(dme) in THF (see; **Figure S1**). The structure of **2** was unambiguously determined by X-ray crystallography, which revealed a square-planar geometry around the Ni center (**Figure 2**). In addition, the geometric index τ_δ for **2** was 0.09, which further supports its square-planar geometry.[10] The ^{1}H NMR spectrum of **2** in benzene-d_6 showed sharp signals within the diamagnetic region (9.29 to 1.0 ppm), which is consistent with the solid-state geometry, as determined by X-ray crystallography (**Figure 2**). The use of the tridentate ligand stabilized the quasi-square-planar geometry of the Ni complex **2**. These results suggest that **1** holds promise as a precursor for T-shaped Ni(I) complexes with metalloradical features. Finally, reduction of **2** with KH in THF resulted in a color change from dark green to dark blue and afforded **1** as a deep blue solid (optimization, see; Table S**1**). The ^{1}H NMR spectrum of **1** in benzene-d_6 was silent, with no peaks assignable to dimers containing Ni–Ni and Ni–C bonds were observed, which indicates the effective steric protection around the reactive Ni center by bulky substituents. Complex **1** remained stable at −35 °C in the solid state as well as in either toluene or THF solutions for at least a week under a N_2 atmosphere. However, exposure of a toluene solution of **1** to air resulted in immediate decomposition. The electronic absorption spectrum of **1** in toluene displayed a broad absorption band at ~680 nm (**Figure 3**, red), which was not observed in the spectra of precursor **2** (blue).

Figure 2 ORTEP drawing of **2** with 50% probability ellipsoids. Hydrogen atoms are omitted for clarity. Single diastereomer is shown.

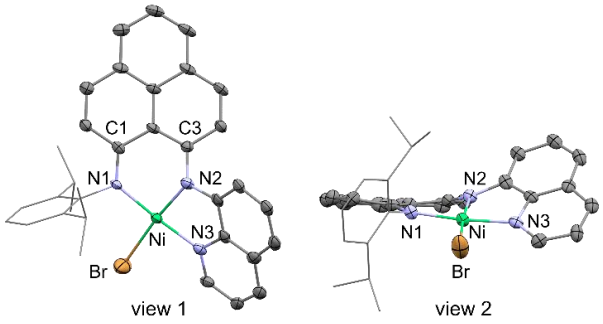

Figure 3 Electronic absorption spectra of **1** (red) and **2** (blue) (1.0×10^{-4} M in toluene).

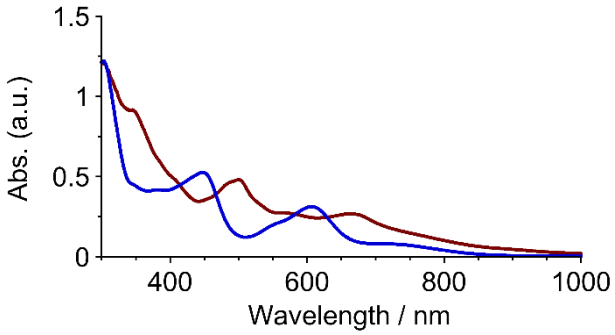

Density functional theory (DFT) calculations at the UM06[11]/def2TZVPP[12] level estimated a small difference in the lengths of C1−N1 (1.320 Å) and C3−N2 (1.338 Å) bonds in **1**, suggesting the delocalization of anionic properties through the π system of phenalenyl similar to that observed in **2** (**Figure 4**). The calculation also indicates that the singly occupied molecular orbital (SOMO) of **1** is predominantly located on the $d_{x^2-y^2}$ orbital of nickel, which contributes to its T-shaped geometry. In contrast, the lowest unoccupied molecular orbital (LUMO) is primarily distributed across the π orbital of the ligand. Unlike the SOMO and LUMO, which are localized across either the metal or the ligand, SOMO-1 is composed of contributions from both the d_{z^2} orbital of the nickel and the π orbital of the ligand. Time-dependent (TD)-DFT calculations at the TD-UM06/def2TZVPP//UM06/def2TZVPP level indicate that the broad absorption band of **1** at ~700 nm is assignable to the SOMO-1 to LUMO ($f = 0.003$) transition.

Figure 4 DFT calculations: (a) Selected molecular orbitals of **1** calculated at the UM06/def2TZVPP level. (b) Selected frontier orbitals of **1** calculated at the TD-UM06/def2TZVPP//UM06/def2TZVPP level.

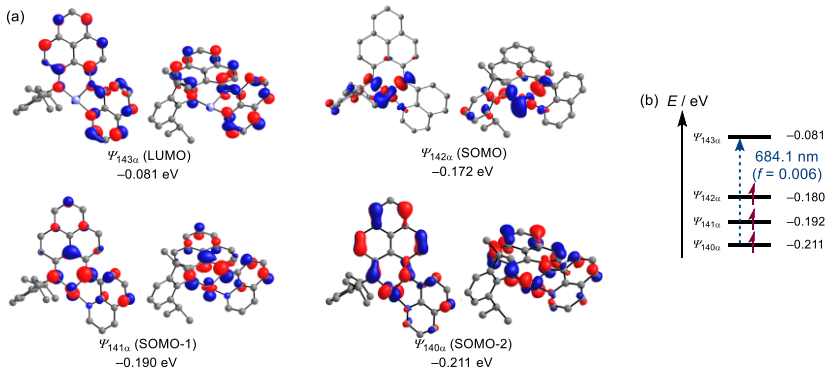

Figure 5 (a) Observed (top, red, 1×10^{-4} M in toluene, $g_1 = 2.29$, $g_2 = 2.15$, $g_3 = 2.03$, and $A_{N3} = 1.52$ mT) and simulated (bottom, black) ESR spectra of **1** in toluene at 110 K. (b) Determined HFCCs (in G) of **1**. In parentheses, HFCCs were estimated using the UM06/def2TZVPP method and the McConnell model. (c) The spin density map of **1** calculated using the UM06/def2TZVPP method depicts at contour value = 0.01.

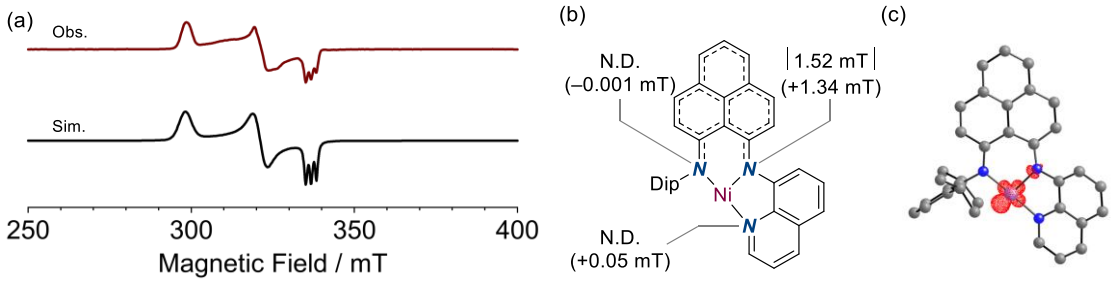

Figure 6 (a) Ni K-edge XANES spectra of **1** (red) and **2** (blue) (2×10^{-2} M in THF), nickel foil (green dot), and NiO (black dot). (b) Fourier-transformed Ni K-edge EXAFS spectra of **1** (red) and **2** (blue).

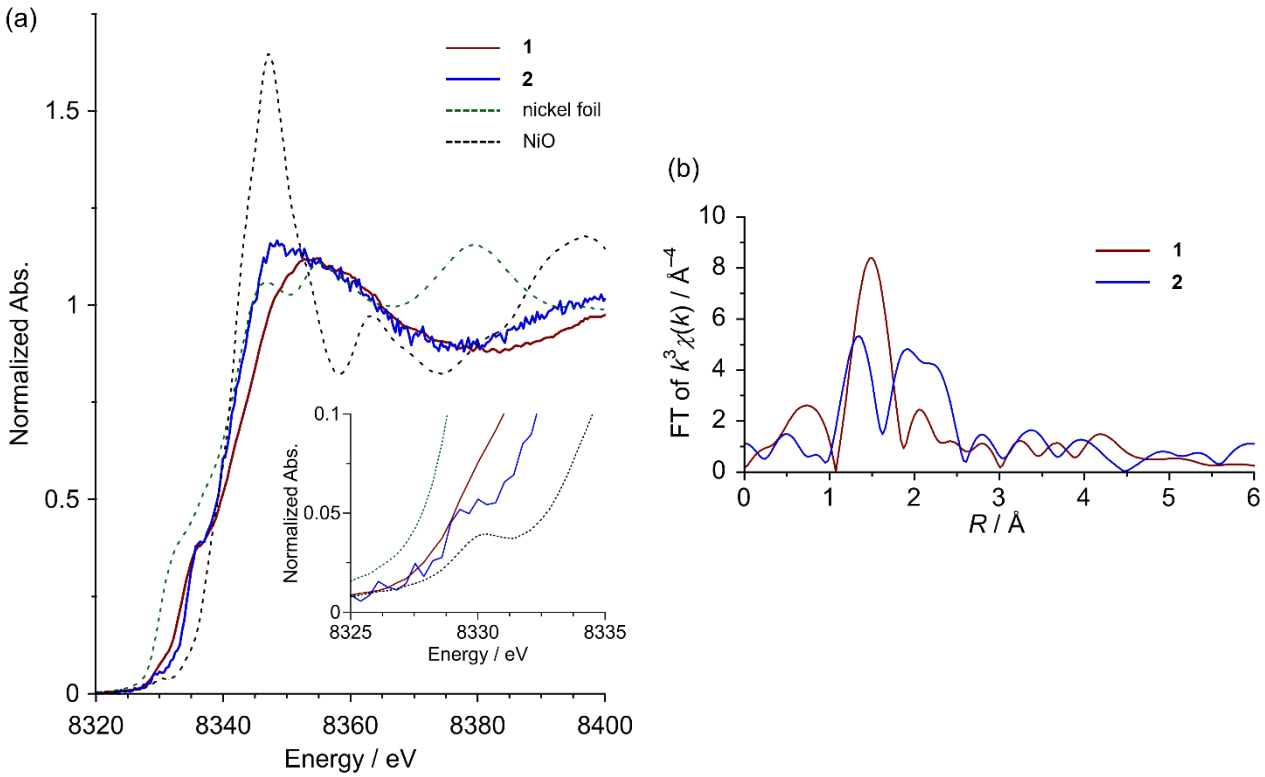

To elucidate the spin structure of **1**, X-band electron spin resonance (ESR) measurements were performed. The ESR spectrum of **1** in frozen toluene at 110 K revealed a rhombic *g*-tensor (**Figure 5a**), which is simulated as an $S = 1/2$ spin system with *g* values of $g_1 = 2.29$, $g_2 = 2.12$, and $g_3 = 2.03$ and an A_{N3} value of 1.52 mT (**Figure 5b**), which approximate the results observed for Lee's T-shaped Ni(I) complex.[7b] Mulliken population analysis suggests that ~85% of the spin is localized on the Ni center. These experimental findings, coupled with theoretical calculations, indicate that complex **1** could be characterized as a metalloradical, with spin density distributed on the $d_{x^2-y^2}$ orbital of the nickel center (**Figure 5c**).

To further elucidate the structural characteristics of **1**, X-ray absorption fine structure (XAFS) studies were performed. Ni K-edge XAFS measurements of both **1** and **2** in THF were conducted in fluorescence mode at 300 K (**Figure 6a**). X-ray absorption near-edge structure (XANES) spectra indicate that the photon energy of **1** appears to correspond to a Ni(I) species, because it is lower than that of **2** albeit higher than that of nickel foil. Additionally, the pre-edge peak ~8,330 eV in the XANES spectrum of **4** also suggests a Ni(II) species (see the inset of **Figure 6a**; *cf.* **Figure S2**).[13] To evaluate the structures of complexes **1** and **2**, the extended EXAFS regions were analyzed (**Figure 6b**). A curve-fitting analysis of **2** by the Fourier transformed EXAFS (FT-EXAFS) data revealed the presence of two types of chemical bonding, Ni–Br and Ni–N, which suggests that complex **2** is a four-coordinated complex. The bond length and coordination number derived from the EXAFS spectrum of **2** were in good agreement with the corresponding structure obtained from X-ray crystallography (**Table 1**). Analysis of the EXAFS spectrum of **1** indicated the presence of three Ni–N bonds with bond lengths similar to those of **2**. These XAFS analyses suggest that complex **1** is a three-coordinated Ni(I) species.

Table 1 Structural Parameters Obtained by Curve-Fitting Analysis of the Ni K-edge FT-EXAFS spectra.[a]

	bond	CN	*r* (Å)	DW(σ^2) (Å^2)	*R* (%)
2	Ni–N	3.2(4)	1.87(5)	0.012(7)	13.9
	Ni–Br	1.0(1)	2.37(4)	0.004(3)	
1	Ni–N	3.4(3)	1.87(4)	0.004(3)	13.4

[a]CN: Coordination Number; DW: Debye–Waller factor.

We next investigated the reactivity of **1** (**Scheme 2**). The distinguishing feature of T-shaped Ni(I) complexes is their metalloradical reactivity.[5,6,7] The reaction of **1** with CH_2Br_2 yielded bromide complex **2**, which indicates that a halogen atom transfer reaction occurred at the Ni center, a phenomenon that has previously been reported for other Ni(I) complexes.[14] Complex **1** also reacted with PhSSPh at the Ni center to form sulfide complex **4** with the formation of a Ni–S bond. Upon reacting **1** with MeI, both Ni‑Me **5** and Ni‑I **6** complexes were formed in approximately equal ratios, which further demonstrates its metalloradical behavior.

Scheme 2 Reactivity of nickel metalloradical 1. Reaction conditions: (a) KH (3.5 equiv), THF, rt, 15 h. (b) CH_2Br_2 (1.2 equiv), toluene, 15 h, rt. (c) PhSSPh (1.3 equiv), toluene, rt, 15 h. (d) MeI (4.0 equiv), toluene, rt, 15 h (**5** : **6** = 1 : 1). The overall yields for two-step reactions from **2** are shown.

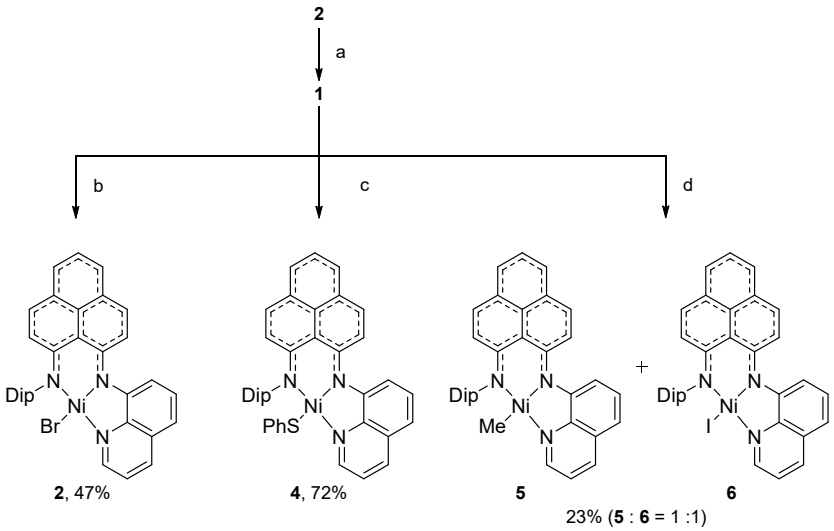

2.3. Conclusion

In summary, herein we report the synthesis and characterization of a Ni(I) complex featuring a newly developed PLY-based tridentate ligand. Through spectroscopic and reactivity studies, we identified the metalloradical nature of **1**. Further exploration of the unique reactivity stemming from its metalloradical characteristics is currently underway in our laboratory.

2.4. Experimental Section

I. General Information.

^{1}H and ^{13}C NMR spectra were recorded on a JEOL ECS-400 spectrometer and JEOL ESZ-400S spectrometer. The chemical shifts were recorded relative to $CHCl_3$(δ: 7.26 for ^{1}H NMR in $CDCl_3$), $CDCl_3$(δ: 77.16 for ^{13}C NMR in CDCl3), benzene (δ: 7.16 for ^{1}H NMR in benzene-d_6), benzene-d_6 (δ: 128.06 for ^{13}C NMR in benzene-d_6) CH_2Cl_2 (δ: 5.32 for ^{1}H NMR in CD_2Cl_2), CD_2Cl_2 (δ: 53.84 for ^{13}C NMR in CD_2Cl_2) or THF-d_8 (δ: 25.31 for ^{13}C NMR in THF-d_8) as an internal or external standard. Data are recorded as follows: chemical shifts in ppm (δ), multiplicity (s = singlet, d = doublet, dd = double doublet, t = triplet, brs = broad singlet, sep = septet, m = multiplet), coupling constant (Hz), and integration. Infrared spectra (IR) were obtained using a JASCO FT/IR-4200 spectrometer. Absorption is reported in reciprocal centimeters (cm^{-1}) with the following relative intensities: s (strong), m (medium), or w (weak). High resolution mass spectra (HRMS) were obtained using a JEOL JMS-T100LP spectrometer. Elemental analyses were performed on a J-Science Lab. Co. MICRO CORDER JM10 elemental analyzer. Melting points were determined on a Stanford Research Systems MPA100 apparatus equipped with a digital thermometer and are uncorrected. ESR spectra were recorded on a Bruker EMXmicro spectrometer and Bruker Magnettech ESR5000 spectrometer, and were simulated with the EasySpin software program.[15] Electronic absorption spectra were recorded on a JASCO V-770 spectrophotometer. Ni K-edge XAFS measurements were conducted at BL01B1 beamline in SPring-8 facility of the Japan Synchrotron Radiation Research Institute. After monochromatizating the incident X-ray beam by a Si(111) double crystal monochromator, energy was calibrated using Cu foil. Ni K-edge XAFS of the solution samples were measured in fluorescence mode. XAFS data was analyzed by xTunes software.[16] X-ray crystal

analyses were performed on a Rigaku/XtaLABPro P200 Hybrid Photon Counting diffractometer (Cu-Kα, λ = 1.54184 Å). The structures were solved with olex2.solve 1.5 and refined with SHELXL−2018/3).

II. Materials.

All commercially available reagents and solvents were supplied from TCI, WAKO and Aldrich. The ligand [3059559-13-3],[9] $NiBr_2$(dme) [CAS: 28923-39-9][17] NiI_2(dme) [CAS: 1412442-55-7][18] were prepared according to literature procedure. All reactions with moisture- or air-sensitive compounds were performed in a nitrogen- or argon-filled glove box.

III. Synthesis of Ni(I) complex.

Synthesis of 2.

A THF solution of the ligand (0.72 g, 1.5 mol) in 10 mL was cooled at freezer (–35 °C) for 10 minutes, then KHMDS (1.0 M in THF) (1.8 mL, 1.8 mmol) was added to the solution and stirred at rt for 3 h under a nitrogen atmosphere. The mixture was cooled at freezer (–35 °C) for 10 minutes and then, $NiBr_2$(dme) (0.57 g, 1.9 mmol) was added to the solution and stirred at 65 °C for 15 h. The resulting mixture was filtered off to remove insoluble part and the filtrate was concentrated under reduced pressure. The residual solid was washed with hexane and dried under reduced pressure to give a desired product **2** as a dark green solid (0.80 g, 1.3 mmol, 86%). Two diastereomers were obtained in a ratio of 82:18 determined by ^{1}H NMR. Single crystals suit for crystallographic analysis were obtained by slow evaporation of benzene solution.

Mp >300 °C.

^{1}H NMR ($CDCl_3$, 400 MHz) δ: 9.29 (d, J = 4.6 Hz, 1H, major), 8.94 (d, J = 4.6 Hz, 1H, minor), 8.22–8.18 (m, 1H+1H, major and minor) 8.10 (d, J = 9.2 Hz, 1H+1H, major and minor), 7.90–7.85 (m, 1H+1H, major and minor), 7.80–7.74 (m, 1H+1H, major and minor), 7.71 (d, J = 7.3 Hz, 1H+1H, major and minor), 7.65 (d, J = 7.3 Hz, 1H+1H, major and minor), 7.45–7.40 (m, 2H+2H, major and minor), 7.36–7.24 (m, 4H+4H, major and minor), 7.21–7.16 (m, 4H+4H, major and minor) 6.53–6.48 (m, 1H+1H, major and minor), 4.22 (brs, 1H+1H, major and minor), 1.68 (brs, 6H+6H, major and minor), 1.04 (d, J = 6.4 Hz, 6H+6H, major and minor).

^{13}C NMR (THF-d_8, 101 MHz) δ: 156.5, 155.9, 152.5, 149.4, 149.3, 145.2, 143.1, 139.2, 134.3, 133.4, 130.3, 129.8, 128.6, 128.5, 127.7, 127.0, 126.5, 124.0, 123.8 (two peaks were overlapped), 123.4, 123.0, 122.5, 120.2, 118.5, 118.1, 29.6, 24.7, 24.6.

IR (KBr, cm^{-1}): 3056 w, 2958 m, 2927 w, 2866 w, 1624 m, 1575 m, 1559 m, 1502 m, 1484 s, 1462 m, 1425 m, 1410 m, 1380 m, 1336 s, 1318 m, 1282 w, 1248 m, 1185 m, 1159 m, 1099 w, 1055 w, 963 w, 839 m, 823 m, 804 w, 780 m, 764 m, 691 m, 594 w, 494 w.

HRMS (DART+) m/z $[M+H]^+$ Calcd for $C_{34}H_{31}N_3{}^{58}Ni^{79}Br^+$: 618.1049, found: 618.1074.

Elemental Anal. Calcd. for $C_{34}H_{30}N_3NiBr$: C, 65.95 H, 4.88; N, 6.79. Found: C, 66.28; H, 5.55; N, 6.48. The higher observed H value might be due to the contamination of the ligand generated by decomposition of **2** during the operation.

Synthesis of 1.

A mixture of **2** (310 mg, 0.50 mol) and KH (30% in mineral oil) (243 mg, 1.76 mol) in THF (5.0 mL) was stirred at room temperature for 15 h under nitrogen atmosphere. The resulting mixture was filtered off to remove insoluble part and the filtrate was concentrated under reduced pressure. The residual solid was dissolved in benzene and filtered off to remove insoluble part. The filtrate was then concentrated under reduced pressure to give **1** as a dark blue solid (265 mg).

Mp >300 °C.

IR (KBr, cm^{-1}): 3056 w, 2958 m, 2925 m, 2863 w, 1626 m, 1578 m, 1556 m, 1486 m, 1463 m, 1420 m, 1380 m, 1337 s, 1320 m, 1248 w, 1182 m, 1158 m, 1098 w, 1056 w, 960 w, 837 w, 758 w, 692 w.

HRMS (ESI+ in MeCN) *m/z* [M+H]+ Calcd for $C_{34}H_{31}N_3{}^{58}Ni$: 539.1866, found: 539.1842.

Magnetic moment by Evans' method[19]: μ_{eff} = 1.33. (*cf.* theoretical value $\mu = \sqrt{3}\mu B$)

Table S1 Reductant screening.

entries	reductant	solvent	yield(%)
1	KC_8	toluene	0
2	KC_8	THF	0
3	$KBEt_3H$	toluene	ca. 60[a]
4	KH	toluene	0
5	KH	THF	98[b]

[a]containing unseparable impurities.
[b]based on weight

IV. Reactivity of Ni(I) complex.

Reaction of 1 with CH_2Br_2.

CH_2Br_2 (44 mg, 0.25 mmol) was added to a suspension of **1** (103 mg, 0.17 mmol) in toluene (2.0 mL), and the mixture was stirred at room temperature for 15 h. The resulting heterogeneous mixture was filtered, and the insoluble materials were carefully washed with toluene until the color of the filtrate became colorless (ca. 20 mL). The resulting filtrate was then concentrated under reduced pressure to give a solid, which was washed with hexane and dried under reduced pressure, producing the desired product **2** as a dark green solid (55 mg, 47% overall yield from **2**).

Reaction of 1 with PhSSPh.

PhSSPh (28 mg, 0.13 mmol) was added to a suspension of **1** (52 mg, 0.010 mmol) in toluene (1.0 mL) solution and the mixture was stirred at room temperature for 15 h. The resulting heterogeneous mixture was filtered, and the insoluble materials were carefully washed with toluene until the color of the filtrate became colorless (ca. 20 mL). The resulting filtrate was then concentrated under reduced pressure to give a solid, which was washed with hexane and dried under reduced pressure, producing the desired product **4** as a brown solid. (45 mg, 72% overall yield from **2**).

Alternative synthetic method of **4**: Phenylthiotrimethylsilane (TMSSPh) (88 mg, 0.48 mmol) was added to a 3 mL THF solution of **2** (190 mg, 0.31 mmol) and CsF (57 mg, 0.38 mmol). Then, the mixture was stirred at room temperature for 15 h under dark situation. The resulting mixture was filtered off with THF to remove insoluble impurities and the filtrate was concentrated under reduced pressure. The residual solid was washed with hexane and dried under reduced pressure to give a desired product **4** as a brown solid. (28 mg, 0.044 mmol, 14%). Analytically pure sample was obtained by recrystallization from THF/hexane solution.

Mp > 300 °C

^{1}H NMR (benzene-d_6, 400 MHz) δ: 9.53 (d, J = 5.3 Hz, 1H), 7.78 (d, J = 9.2 Hz, 1H), 7.52 (d, J = 7.8 Hz, 1H), 7.31-7.18 (m, 7H), 7.16–7.07 (m, 6H) (Some signals were overlapped with solvent peak), 6.82–6.77 (m, 2H), 6.69 (d, J = 9.6 Hz, 1H), 6.58 (d, J = 8.2 Hz, 1H), 6.24 (dd, J = 8.2, 5.3 Hz, 1H), 4.45 (brs, 2H), 1.94 (d, J = 6.0 Hz, 6H), 1.13 (d, J = 6.9 Hz, 6H)

^{13}C NMR (CD_2Cl_2, 101 MHz) δ: 156.1, 155.1, 152.1, 149.1, 149.0, 148.8, 145.0, 143.3, 138.8, 138.7, 134.1, 133.2, 130.1, 130.0, 129.3, 128.3, 128.2, 127.2, 126.5, 126.4, 123.8(two peaks were overlapped), 123.5, 123.3, 122.6, 122.3, 119.8, 118.2, 118.1, 118.0, 29.4, 24.73, 24.65.

IR (KBr, cm^{-1}): 3056 w, 2959 w, 2925 w, 2866 w, 1626 s, 1576 s, 1502 w, 1483 s, 1463 m, 1425 m, 1410 m, 1380 s, 1335 s, 1317 m, 1282 w, 1248 m, 1184 m, 1157 m, 1098 w, 962 w, 839 m, 822 m, 780 m, 762 m, 741 m, 691 m, 580 w, 526 m.

HRMS (DART+) m/z $[M+H]^+$ calcd for $C_{40}H_{36}N_3{}^{58}NiS^+$: 648.1978, found: 648.2007.

Reaction of 1 with MeI.

MeI (28 mg, 0.20 mmol) was added to a suspension of **1** (29 mg, 0.050 mmol) in toluene (0.5 mL) and the mixture was stirred at room temperature for 15 h. The resulting heterogeneous mixture was filtered, and the insoluble materials were carefully washed with toluene until the color of the filtrate became colorless (ca. 20 mL). The resulting filtrate was then concentrated under reduced pressure to give a solid, which was washed with hexane and dried under reduced pressure, producing the product mixture **6** and **7** as a dark green solid. (7.0 mg, 23% overall yield from **2**; **5** : **6** = 1 : 1, based on ^{1}H NMR).

Alternative synthetic method of **5**: MeMgBr (3 M in THF) (0.07 mL, 0.21 mmol) was added to a 2.0 mL THF solution of **2** (130.9 mg, 0.21 mmol) and the mixture was stirred at room temperature for 15 h under dark conditions. The resulting mixture was filtered off with THF to remove insoluble impurities and the filtrate was concentrated under reduced pressure. The residual solid was washed with hexane and dried under reduced pressure to give a desired product **5** as a dark red solid. (50 mg, 0.092 mmol, 43%).

Mp > 300 °C.

^{1}H NMR (400 MHz, benzene-d_6) δ: 8.21 (d, J = 4.6 Hz, 1H), 7.95 (d, J = 9.2 Hz, 1H), 7.56 (d, J = 6.9 Hz, 1H), 7.47 (d, J = 8.0 Hz, 1H), 7.42 (d, J = 10.3 Hz, 1H), 7.38 (d, J = 6.9 Hz, 1H), 7.29–7.21 (m, 4H), 7.12 (t, J = 7.5 Hz, 1H), 6.98–6.92 (m, 2H), 6.71–6.66 (m, 2H), 6.36 (dd, J = 8.0, 4.6 Hz, 1H), 4.26 (brs, 2H), 1.54 (d, J = 6.8 Hz, 6H), 1.10 (d, J = 6.4 Hz, 6H), –0.21 (s, 3H).

^{13}C NMR (benzene-d_6, 101 MHz) δ: 157.1, 152.7, 149.0, 148.5, 148.4, 145.8, 142.3, 136.8, 132.4, 132.0, 129.7,

129.1, 128.82, 128.79, 127.6, 127.0, 126.0, 124.9, 124.1 (two peaks were overlapped), 122.5, 122.1, 121.5, 118.4, 116.7, 116.4, 28.7, 24.8, 24.3, 0.9.

IR (KBr, cm^{-1}): 3048 s, 3235 m, 3056 w, 2959 m, 2866 w, 1629 s, 1577 m, 1556 m, 1503 m, 1485 m, 1410 m, 1380 m, 1335 s, 1319 m, 1247 w, 1182m, 1156 m, 1056 w, 961 w, 837 w, 819 w, 802 w, 779 w, 753 w, 691 w.

HRMS (DART+) *m/z* $[M+H]^+$ calcd for $C_{35}H_{34}N_3{}^{58}Ni^+$ 554.2122, found: 554.2101.

Alternative synthetic method of **6**: A THF solution (4.8 mL) of the ligand (367 mg, 0.76 mol) was cooled at freezer (–30 °C) for 10 minutes, then KHMDS (1.0 M in THF) (0.9 mL, 0.9 mmol) was added to the solution and stirred at rt for 3 h under a nitrogen atmosphere. The mixture was cooled at freezer (–30 °C) for 10 minutes, then NiI_2(dme) (288 mg, 0.72 mmol) was added to the solution and stirred at 65 °C for 15 h. The resulting mixture was filtered off to remove insoluble impurities and the filtrate was concentrated under reduced pressure. The residual solid was washed with hexane and dried under reduced pressure to give a desired product **6** as a dark green solid (191 mg, 0.29 mmol, 38%).

Mp > 300 °C

^{1}H NMR (benzene-d_6, 400 MHz) δ: 10.19 (dd, J = 5.3, 1.1 Hz, 1H), 7.72 (d, J = 9.2 Hz, 1H), 7.56 (dd, J = 7.6, 1.1 Hz, 1H), 7.38 (d, J = 9.2 Hz, 1H), 7.34–7.28 (m, 3H), 7.22–7.17 (m , 1H), 7.14–7.08 (m , 1H), 7.09–7.04 (m, 2H), 6.90-6.84 (m, 2H), 6.59 (d, J = 9.6 Hz, 1H), 6.52 (d, J = 8.2 Hz, 1H), 6.29 (dd, J = 8.2, 5.5 Hz, 1H), 4.70 (brs, 2H), 1.92 (d, J = 6.4 Hz, 6H), 1.10 (d, J = 6.9 Hz, 6H).

^{13}C NMR (CD_2Cl_2, 101 MHz) δ: 159.4, 151.0, 145.0, 144.9, 144.3, 139.0, 133.9, 133.0, 132.9, 129.9, 129.8, 129.4, 128.2, 127.7, 127.5, 127.4, 126.9, 126.7, 124.4, 124.3, 124.1 (two peaks are overlapped), 123.8, 123.8, 120.4, 119.6, 29.4, 25.1, 24.7.

IR (KBr, cm^{-1}): 3051 m, 2957 m, 2925 m, 2866 m, 1624 s, 1577 s, 1558 s, 1522 s, 1501 s, 1485 s, 1501 s, 1485 s, 1463 s, 1423 s, 1408 s, 1334 s, 1281 m, 1249 m, 1182s, 1154 s, 1102 m, 1055 w, 960 m, 839 m, 817 s, 778 s, 690 m, 633 w, 580 w.

HRMS (DART+) *m/z* $[M+H]^+$ calcd for $C_{34}H_{31}N_3{}^{58}Ni^{126}I^+$: 666.0911, found: 666.0942.

V Electronic Absorption Spectra.

10 mm quartz cell equipped with ground glass stopper or screw cap in a glove box was using for measurement. Electronic absorption spectra measurements for **1** and **2** were recorded in toluene (1.0×10^{-4} M) at 25 °C.

VI. Crystallographic Information.

Figure S1 (a) ORTEP drawing of **2**. (b) Crystal Packing of **2**.

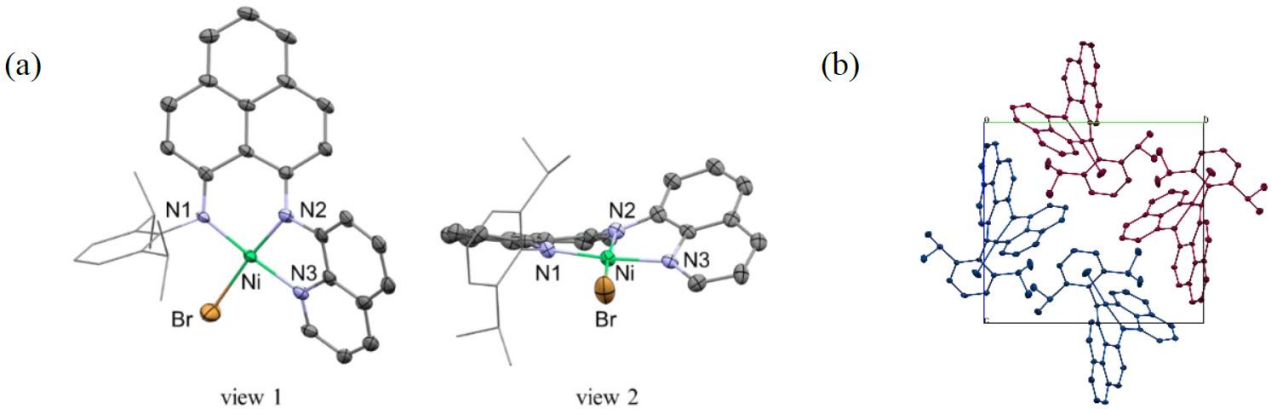

[a]Crystal data for **2**, monoclinic, space group $P\,2_1/c$ (no. 14), a = 16.4893(8) Å, b = 13.5321(5) Å, c = 12.7016(5) Å, β = 103.346(4)°, V = 2757.63(19) Å3, T = 123 K, Z = 4, $R1$ ($wR2$) = 0.0933 (0.2486) for 356 parameters and 5373 unique reflections. GOF = 1.090. CCDC 2344998.

VII. K-edge XANES spectra.

Figure S2 Pre-edge peaks in K-edge XANES spectra of **2** (blue) (2 × 10^{-2} M in THF), NiO (black dot).

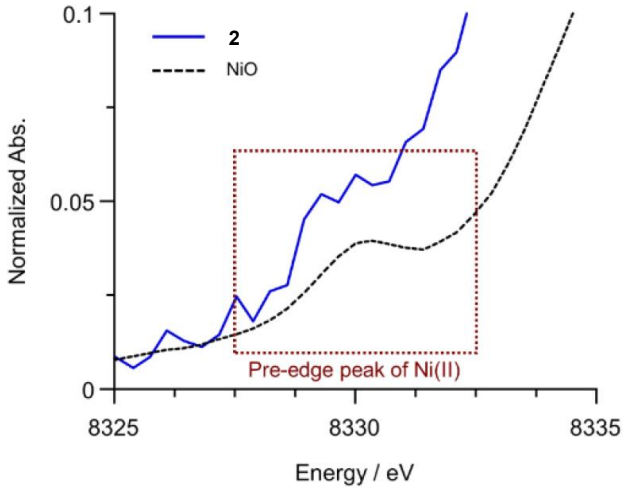

VIII. Computational Details .

All calculations were conducted using the Gaussian 16 suite program (G16 Rev C.01).[20] Optimization and HFCCs estimation were performed at the UM06/def2TZVPP level of approximation. Harmonic vibration frequency analysis was conducted with the optimized structures at the same level of theory to verify all stationary points as local minima (with no imaginary frequency). Each reported minimum has zero imaginary frequency. All structures, orbitals and spin density maps were visualized by GaussView 6.1.1[21] and Chemcraft Version 1.8.[22]

IX. Selected Structural Properties of 2 and 1

Table S2 Selected bond lengths (Å) and bond angles (degree) for **2** and **1**.

	2 (crystal)	**2** (calc.)[a]	**1** (calc.)[a]
N1–Ni	1.903(5)	1.915	1.866
N2–Ni	1.870(5)	1.887	1.945
N3–Ni	1.939(5)	1.968	1.930
X–Ni	2.330(1)	2.336	-
N1–C1	1.350(8)	1.318	1.320
N2–C3	1.359(8)	1.348	1.338
N1–Ni–N3	173.4(2)	167.0	174.8
N2–Ni–X	173.5(2)	169.7	-

[a]The structures of **2** and **1** were optimized using the UM06/def2TZVPP level of theory.

Table S3 Selected WBIs for **2** and **1**.

	2 (calc.)[a]	**1** (calc.)[a]
N1–Ni	0.479	0.346
N2–Ni	0.474	0.282
N3–Ni	0.406	0.315
X–Ni	0.761	-
N1–C1	1.473	1.434
N2–C3	1.257	1.316

[a]The structures of **2** and **1** were optimized using the UM06/def2TZVPP level of theory.

X. Cartesian Coordinates and Energies of Optimized Structures.

1

Ni	-1.07303300	0.63349900	-0.34961600	C	2.98878700	0.18368700	0.46763900
N	-2.98850300	0.50589200	-0.54877300	H	3.21747500	1.22531700	0.65142900
N	-1.12582900	-1.27926400	-0.00041600	C	-3.42125900	-0.72038800	-0.14349100
N	0.75120600	0.82631000	-0.00612000	C	-0.20558700	-3.43369200	-0.53680400
C	1.33080700	4.15595800	1.48699600	H	-1.19700800	-3.77057300	-0.80283600
H	1.27626100	4.64469500	2.45302700	C	-2.41945800	-1.69272800	0.18571500

C	1.62211300	-0.15159600	0.15675800	C	-4.79566600	-1.00906300	-0.01542900
C	1.67193100	4.89572300	0.37046100	C	-5.70655400	-0.00731900	-0.39931200
H	1.88614500	5.95301700	0.46299300	H	-6.76915900	-0.20866600	-0.32614200
C	0.83106500	-4.28980900	-0.61698900	C	-5.24890900	1.19976000	-0.84322700
H	0.67085400	-5.31663700	-0.92743400	H	-5.92707900	1.98751300	-1.14052200
C	2.64753600	2.72478800	-3.24034300	C	4.49771700	-4.37307100	-0.04587400
H	2.56441000	3.77709000	-3.52149600	H	5.31146900	-5.08590900	-0.05137000
H	2.67118700	2.14635000	-4.16554100	C	3.96702000	-0.73579900	0.50899800
H	3.60241700	2.58796400	-2.72966800	H	4.98558900	-0.44064600	0.73667800
C	2.36399300	-2.49636200	-0.02736700	C	3.70316900	-2.10509100	0.23611300
C	2.14728300	-3.86950600	-0.30999000	C	-2.86870900	-2.87379900	0.75596600
C	-0.05100400	-2.06134000	-0.15341900	H	-2.15272200	-3.59967500	1.11494900
C	1.28728600	-1.55588800	-0.00818800	C	3.20900000	-4.77514300	-0.32155100
C	1.05212200	2.79930900	1.39486500	H	2.99554800	-5.81248000	-0.55434000
C	-3.86847700	1.42425900	-0.88465300	C	-4.23500400	-3.14308300	0.90745900
H	-3.47137800	2.38605700	-1.19068100	H	-4.52882900	-4.08610000	1.35191500
C	1.11985300	2.18844200	0.13361800	C	0.62667800	2.02064800	2.61746700
C	1.47080400	2.92453500	-1.00747100	H	0.71951700	0.95648100	2.38848900
C	1.73851200	4.27913800	-0.86449400	C	4.73309200	-3.03847500	0.23315500
H	2.00469300	4.86359900	-1.73752300	H	5.73792500	-2.69485000	0.45233700
C	-5.19350700	-2.25468100	0.50767400	C	-0.84229000	2.29161900	2.92118700
H	-6.24839600	-2.47575600	0.61043800	H	-1.00054200	3.35014200	3.14444900
C	0.15554000	2.52953800	-3.07378100	H	-1.17727300	1.70969000	3.78233800
H	0.00407800	3.60125100	-3.22867800	H	-1.47207100	2.02738300	2.06604400
H	-0.68327900	2.15170200	-2.47683800	C	1.49421600	2.30407800	3.83364900
H	0.12353600	2.03634300	-4.04745800	H	2.55176700	2.14440200	3.61462100
C	1.48457800	2.27550100	-2.37077800	H	1.21533000	1.64533700	4.65799900
H	1.57984600	1.19674900	-2.22568000	H	1.37643200	3.33077900	4.18757000

Method: UM06/def2TZVPP opt freq

imaginary frequencies: 0

EE + Thermal Free Energy Correction: − 2985.261411 Hartree

2

Br	-1.40826100	-2.37696600	-1.45540500	C	1.44943300	4.28482600	-0.93797000
Ni	-1.03376000	-0.26888000	-0.52118400	H	1.40189900	5.28866300	-1.34532600
N	0.74235300	-0.65832600	0.07847700	C	0.42505300	-2.30426200	1.83577000
N	-2.92188200	0.22967800	-0.70877300	C	-3.95265700	-0.48101000	-1.11464400
N	-0.81290200	1.55061900	-0.07270100	H	-3.72292100	-1.44532600	-1.55091300
C	-5.27354500	-0.03403400	-0.97955100	C	0.94708800	-1.98870900	0.57677100
H	-6.07582800	-0.66387200	-1.33774400	C	1.82641200	-3.63289100	-2.60606200
C	0.33514500	2.22554800	-0.28032200	H	2.19297100	-3.31276600	-3.58341100
C	3.76565100	-2.56869300	-1.47627900	H	0.74329900	-3.73091500	-2.65947900
H	4.17199300	-3.53924200	-1.18013700	H	2.25452600	-4.61852000	-2.40854900
H	4.12457000	-1.82478000	-0.76524100	C	4.03767000	0.60500200	0.87413700
H	4.17849400	-2.32405300	-2.45716500	H	4.97043700	0.24824700	1.29773600
C	-5.52312300	1.16687700	-0.38334900	C	0.58154500	-3.60048700	2.30861800
H	-6.53682900	1.52474200	-0.24421900	H	0.16958000	-3.86818600	3.27483100
C	2.71388300	3.74607400	-0.59866600	C	-2.00260700	2.18014700	0.22347800
C	2.94599100	-0.17984200	0.90870400	C	0.31511200	3.57513500	-0.75122600
H	3.00308600	-1.16332900	1.35263500	H	-0.64029900	4.00884600	-1.01089100

C	1.64328200	-2.93545800	-0.18603800	H	1.87163100	-1.64497400	-1.85343400
C	-3.15289100	1.44788500	-0.14841200	C	1.78814000	-4.21133700	0.34093700
C	1.58974700	1.61114600	-0.07417900	H	2.32045100	-4.96132000	-0.23223000
C	-4.44828500	1.95495600	0.06387800	C	5.10101100	3.97908500	-0.30427900
C	2.76431700	2.40831200	-0.14257700	H	6.00113900	4.57481000	-0.37599800
C	1.70005200	0.22093700	0.29597800	C	-4.59330900	3.19619900	0.71376000
C	3.88664600	4.50002500	-0.69349400	H	-5.58653400	3.58843800	0.89183400
H	3.82001500	5.51462300	-1.06978000	C	-0.31991900	-1.28762900	2.67164600
C	1.25687200	-4.55077000	1.56990400	H	-0.17703100	-0.30399600	2.21732400
H	1.37195600	-5.55711900	1.95256800	C	0.21562200	-1.20416000	4.09369000
C	4.01380400	1.90348300	0.28979800	H	0.04494300	-2.13080300	4.64589300
C	-3.47784800	3.86938000	1.12905200	H	-0.28485700	-0.40301500	4.64118100
H	-3.58319100	4.80931100	1.65614000	H	1.28881500	-1.00344100	4.10279900
C	5.15382000	2.69035300	0.20553000	C	-1.81683400	-1.57630600	2.66956200
H	6.09440500	2.28046100	0.55590600	H	-2.20763200	-1.63511600	1.65036700
C	-2.18769000	3.37480600	0.89267200	H	-2.36193600	-0.79638200	3.20697500
H	-1.33245400	3.93130000	1.25125800	H	-2.02800600	-2.53177500	3.15654600
C	2.24153500	-2.62489800	-1.54119900				

Method: UM06/def2TZVPP opt freq

imaginary frequencies: 0

EE + Thermal Free Energy Correction: − 5559.381525 Hartree

2.5. References

1. Selected reviews on Ni(I) complex, see; (a) Lin, C.-Y.; Power, P. P.; *Chem. Soc. Rev*. **2017**, *46*, 5347. (b) Diccianni, J.; Lin, Q.; Diao, T. *Acc. Chem. Res.* **2020**, *53*, 906. (c) Day, C. S.; Rentería-Gómez, Á.; Ton, S. J.; Gogoi, A. R.; Gutierrez, O.; Martin, R. *Nat. Catal*. **2023**, *6*, 244. (d) Day, C. S.; Martin, R. *Chem. Soc. Rev.* **2023**, *52*, 6601. (e) Dawson, G. A.; Spielvogel, E. H.; Diao, T. *Acc. Chem. Res.* **2023**, *56*, 3640.

2. Ragsdale, S. W.; *J. Biol. Chem.* **2009**, *284*, 18571

3. Selected examples, see; (a) Eckert, N. A.; Bones, E. M.; Lachicotte, R. J.; Holland, P. L. *Inorg. Chem.* **2003**, *42*, 1720. (b) Bai, G.; Wei, P.; Stephan, D. W. *Organometallics* **2005**, *24*, 5901.

4. Ott, J. C.; Bürgy, D.; Guan, H.; Gade, L. H. *Acc. Chem. Res.* **2022**, *55*, 857.

5. Eckert, N. A.; Dinescu, A.; Cundari, T. R.; Holland, P. L. *Inorg. Chem.* **2005**, *44*, 7702.

6. Ingleson, M. J.; Fullmer, B. C.; Buschhorn, D. T.; Fan, H.; Pink, M.; Huffman, J. C.; Caulton, K. G.; *Inorg. Chem.* **2008**, *47*, 407.

7. (a) Rettenmeier, C.; Wadepohl, H.; Gade, L. H. *Chem. Eur. J*. **2014**, *20*, 9657. (b) Yoo, C.; Lee, Y. *Angew. Chem., Int. Ed*. **2017**, *56*, 9502. (c) Schneck, F.; Ahrens, J.; Finger, M.; Stueckl, A. C.; Wuertele, C.; Schwarzer, D.; Schneider, S. *Nat. Commun*. **2018**, *9*, 1161. (d). Ghannam, J.; Sun, Z.; Cundari , T. R.; Zeller, M.; Lugosan, A.; Stanek, C. M.; Lee, W.-T. *Inorg. Chem.* **2019**, *58*, 7131. (e) Duan, P.-C.; Schulz, R. A.; Römer, A.; Van Kuiken, B. E.; Dechert, S.; Demeshko, S.; Cutsail III, G. E.; DeBeer, S.; Mata, R. A.; Meyer, F. *Angew. Chem., Int. Ed*. **2021**, *60*, 1891. (f) Pahar, S.; Sharma, V.; Raj, K. V.; Sangole, M. P.; George, C. P.; Singh, K.; Vanka, K.; Gonnade, R. G.; Sen, S. S. *Chem. Eur. J*. **2024**, *30*, e202303957.

8. (a) Kodama, T.; Mukai, N.; Tobisu, M. *Inorg. Chem*. **2023**, *62*, 6554. (b) Kodama, T.; Uchida, K.; Nakasuji, C.; Kishi, R.; Kitagawa, Y.; Tobisu, M. *Inorg. Chem*. **2023**, *62*, 7861.

9. Noguchi, H.; Kodama, T.; Kikkawa, S.; Yamazoe, S.; Tobisu, M. *Chem. Lett.* **2024**, *53*, upae236.

10. (a) Yang, L.; Powell, D. R.; Houser, R. P. *Dalton Trans*. **2007**, 955. (b) Reineke, M. H.; Sampson, M. D. Rheingold, A. L.; Kubiak, C. P. *Inorg. Chem.* **2015**, *54*, 3211.

11. Zhao, Y.; Truhlar, D. G. *Theor. Chem. Acc*. **2008**, *120*, 215.

12. (a) Weigend, F.; Ahlrichs, R.; *Phys. Chem. Chem. Phys*. **2005**, *7*, 3297. (b) Weigend, F. *Phys. Chem. Chem. Phys.* **2006**, *8*, 1057. (c) Zheng, J.; Xu, X.; Truhlar, D. G. *Theor. Chem. Acc*. **2011**, *128*, 295.

13. Zhang, N.; Brugger, J.; Etschmann, B.; Ngothai, Y.; Zeng, D. *PLoS One* **2015**, *10*, e0119805.

14. Zovko, C.; Krätschmer, F.; Schmidt, S.; Seifert, T. P.; Gamer, M. T.; Roesky, P. W. *ChemPlusChem* **2022**, *87*, e202200288.

15. Stoll, S.; Schweiger, A. *J. Magn. Reson*. **2006**, *178*, 42.

16. Asakura, H.; Yamazoe, S.; Misumi, T.; Fujita, A.; Tsukuda, T.; Tanaka, T.; *Rad. Phys. Chem.* **2020**, *175*, 108270.

17. Gomes, C. S. B.; Costa, S. I.; Silva, L. C.; Jiménez-Tenorio, M.; Valerga, P.; Puerta, M. C.; Gomes, P. T. *Eur. J. Inorg. Chem*. **2018**, *2018*, 597.

18. Pfirrmann, S.; Limberg, C.; Hoppe, E. *Z. Anorg. Allg. Chem.* **2009**, *635*, 312.

19. Evans, D. F. *J. Chem. Soc.* **1959**, 2003.

20. Frisch, M. J.; Trucks, G. W.; Schlegel, H. B.; Scuseria, G. E.; Robb, M. A.; Cheeseman, J. R.: Scalmani, G.; Barone, V.; Mennucci, B.; Petersson, G. A.; Nakatsuji, H.; Caricato, M.; Li, X.; Hratchian, H. P.; Izmaylov, A. F.; Bloino, J.; Zheng, G.; Sonnenberg, J. L.; Hada, M.; Ehara, M.; Toyota, K.; Fukuda, R.; Hasegawa, J.; Ishida, M.; Nakajima, T.; Honda, Y.; Kitao, O.; Nakai, H.; Vreven, T.; Montgomery, Jr., J. A.; Peralta, J. E.; Ogliaro, F.; Bearpark, M.; Heyd, J. J.; Brothers, E.; Kudin, K. N.; Staroverov, V. N.; Keith, T.; Kobayashi, R.; Normand, J.; Raghavachari, K.; Rendell, A.; Burant, J. C.; Iyengar, S. S.; Tomasi, J.; Cossi, M.; Rega, N.; Millam, J. M.; Klene, M.; Knox, J. E.; Cross, J. B.; Bakken, V.; Adamo, C.; Jaramillo, J.; Gomperts, R.; Stratmann, R. E.; Yazyev, O.; Austin, A. J.; Cammi, R.; Pomelli, C.; Ochterski, J. W.; Martin, R. L.; Morokuma, K.; Zakrzewski, V. G.; Voth, G. A.; Salvador, P.; Dannenberg, J. J.; Dapprich, S.; Daniels, A. D.; Farkas, O.; Foresman, J. B.; Ortiz, J. V.; Cioslowski, J.; Fox, D. J. Gaussian, Inc., Wallingford CT, **2016**.

21. Dennington, R.; Keith, T. A.; Millam, J. M.; Semichem Inc., Shawnee Mission, KS, **2016**.

22. G. A. Andirenko, https://www.chemcraftprog.com.

Chapter 3

Cationic Nickel(II) Complexes Bearing a Phenalenyl-Based Tridentate Ligand

3.1. Introduction

Cationic transition metal complexes, composed of a cationic metal center and a non- or weakly-coordinating anion, have been recognized as important class of complexes in the field of organometallic and inorganic chemistry.[1] Compared to electronically neutral complexes, cationic complexes exhibit increased electrophilic properties and lower reduction potentials[2] originating from their positive charge, which makes them widely employed as Lewis acids, catalysts for polymer synthesis and chemical transformations. Their electronic properties and reactivity can be modulated not only by the ligand but also by the counter anions, which promises a higher degree of design freedom.

Recently, we reported a nickel(I) complex[3] (DipQN-PLY)Ni(I) (**Figure 1**)[4] bearing a phenalenyl[5]-based N,N,N-tridentate ligand (H-DipQN-PLY),[6] which exhibits metalloradical properties and reactivities.[7] We envisioned that the corresponding cationic nickel(II) complexes could be accessed from Ni(II) (pseudo)halides (*i.e.* **2**), enabling a deeper, systematic understanding of our ligand system. We report herein on the synthesis of cationic nickel(II) complexes and the characterization of their structures, properties and reactivities.

Figure 1 Representative structures of metal complexes bearing a tridentate DipQN-PLY ligand.

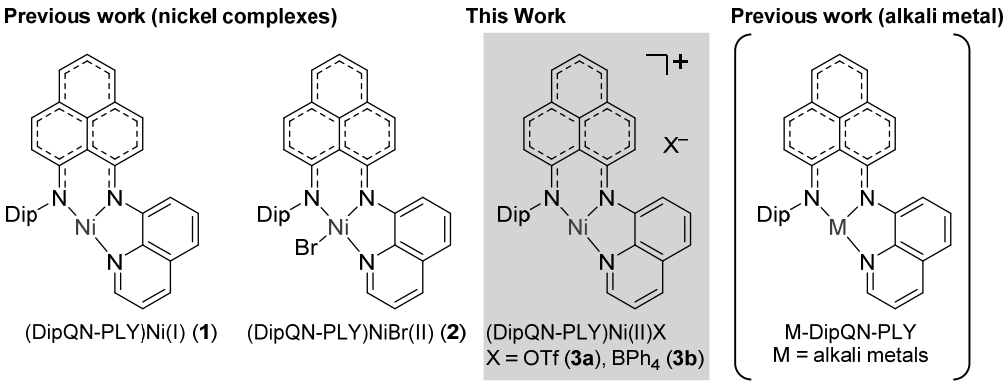

3.2. Results and Discussion

Cationic nickel(II) complex **3a** was synthesized by the rection of the potassium salt (K-DipQN-PLY)[8] with $Ni(OTf)_2$, affording a 53% isolated yield of a dark red solid (**Scheme 1**).[9] The counter anion was then exchanged with BPh_4^- by treatment of $KBPh_4$ in benzene to yield **3b**. Slow evaporation of benzene produced dark red crystals of **3b** that were suitable for X-ray crystallography, which revealed that acetonitrile was coordinated to the nickel center (**Figure 2**). The bond lengths between nickel and the DipQN-PLY ligand are slightly shorter than those in **2**, suggesting stronger electron donation from the ligand to the cationic nickel center, consistent with the positive charge of **3a** (**Table S1**).

Scheme 1 Synthesis of cationic nickel(II) complexes **3**.

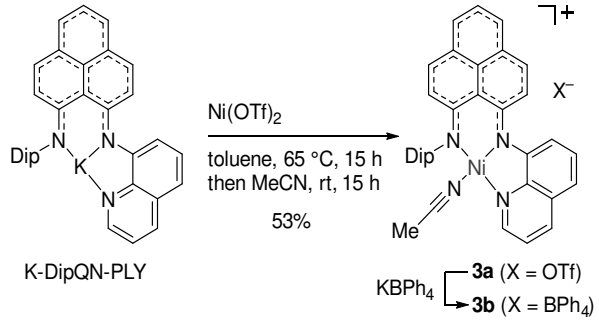

Figure 2 ORTEP drawing of **3b** with 50% probability ellipsoids. Dip group and BPh_4 anion were depicted as wireframe style. Hydrogen atoms are omitted for clarity. One diastereomer is shown. Dip = 2,6-diisopropylphenyl.

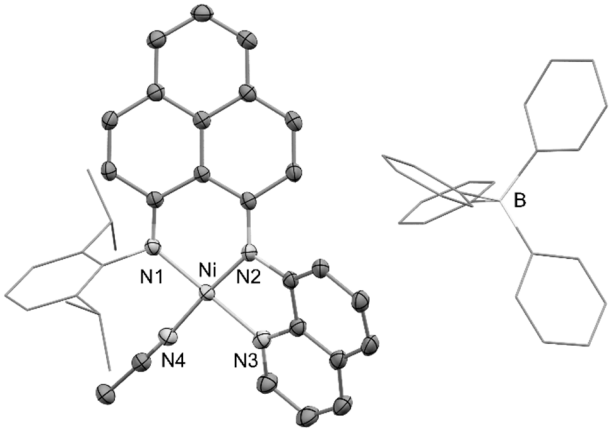

Complex **3a** appears reddish purple in toluene, whereas **2** displays a green color. To investigate the electronic properties in solution, the electronic absorption spectrum of **3a** was measured in toluene (**Figure 3**). Complex **3a** displayed a broad absorption band in the longer wavelength region (~850 nm) and an absorption maximum at 570 nm, with a bathochromic shift of ca. 35 nm compared to that of **2**, along with shoulder bands both at higher energy regions.

Figure 3 Electronic absorption spectra of **3a** (solid) and **2** (dashed) (1.0×10^{-4} M in toluene).

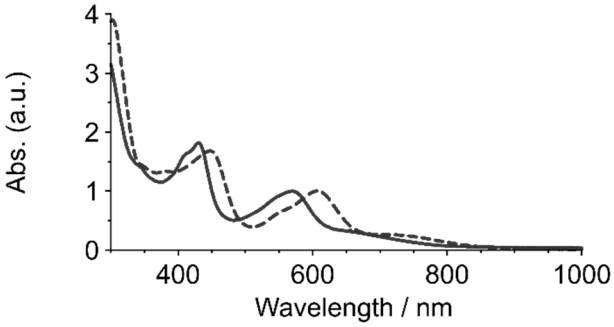

To gain further insights into the electronic properties, density functional theory (DFT) calculations were performed

at the M06[10]/def2TZVPP[11] level of theory. It was predicted that both HOMO and LUMO of **3** were distributed among the π-orbitals of the phenalenyl and quinoline moieties and d-orbital of nickel which were found to be energetically more stable than that for **2**, reflecting electron deficient nature originating the positive charge (**Figure 4a**). The HOMO–LUMO energy gap for **3** (3.23 eV) was 0.18 eV smaller than that of **2** (3.05 eV), which could explain the observed hypochromic shift of **3a** in a qualitative manner. Time dependent(TD)-DFT calculations and natural transition orbital (NTO) analysis[12] revealed that the broad absorption bands observed in **3a** and **2** were assignable to d-d transition on the nickel center, while the strong band at 570 nm was attributed to a combination of metal-to-ligand charge transfer (MLCT) from the nickel center and a π-π* transition of the PLY moiety. The origins of the shoulder bands observed at higher-energy regions appear to differ between **3a** and **2**. For **3a**, the band was assignable to a combination of d-d and π-π* transitions, whereas for **2**, it was attributed to ligand-to-ligand charge transfer from Br to the PLY moiety(**Figure 4b**).

Figure 4 (a) Selected molecular orbitals for **2** and **3**. (b) Natural transition orbitals analysis for **3**.

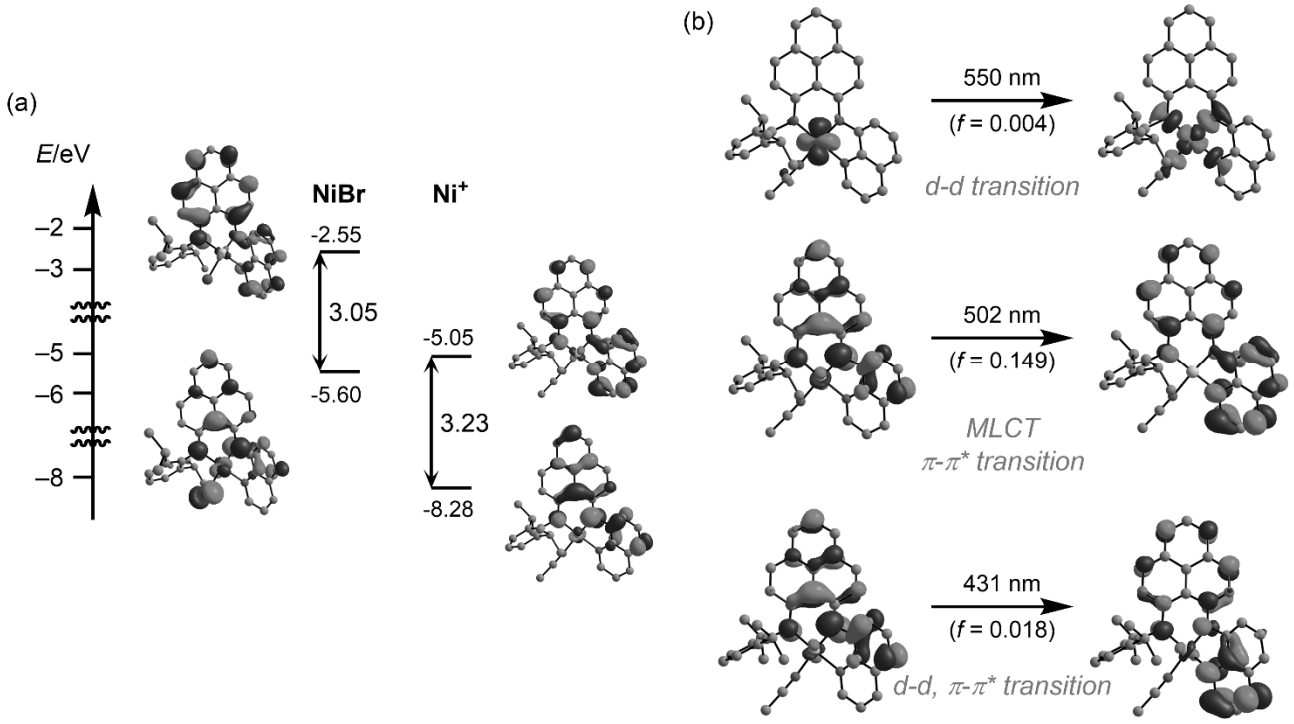

To investigate the redox properties, cyclic voltammetry measurements were conducted for **3a** and **2**. Both complexes exhibited (quasi-)reversible redox processes upon reduction, with the first reduction wave appearing at –1.35 V and –1.65 V vs. Fc/Fc^+ for **3a** and **2**, respectively, and the second reduction occurring at ca. –2.00 V for both (**Figure 5**). The first reduction potential of **3a** was shifted 0.3 V toward the positive side compared to **2**, indicating a lower LUMO level for **3a** due to its positive charge, as predicted by DFT calculations (**Figure 4**). Consistent with this, complex **3a**, unlike **2**, was reduced by Cp^*_2Co(oxidation potential of Cp^*_2Co: −1.91 V vs. Fc/Fc^+ in MeCN)[13] to afford (DipQN-PLY)Ni(I), **1** which can be converted back to **2** through the reaction with CH_2Br_2 in 20% yield (**Scheme 2**).

Figure 5 Cyclic voltammograms of **3a** (solid) and **2** (dashed) (1×10^{-3} M in MeCN containing 1×10^{-1} M $^{n}Bu_4PF_6$) at a scan rate of 100 mV/sec.

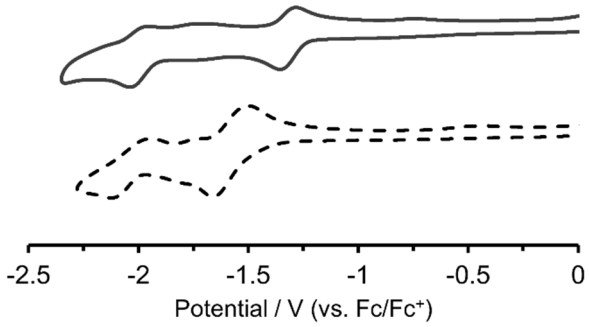

Scheme 2 Reduction of **3a** and oxidation of **1**.

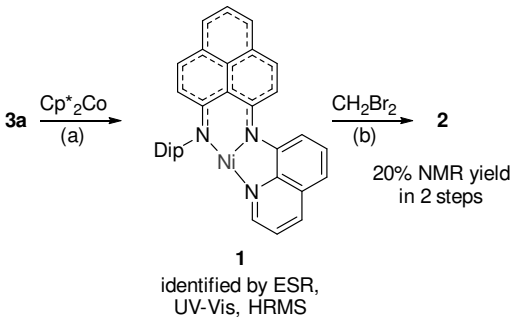

Reaction conditions; (a) **3a** (1.0 equiv), Cp^*_2Co (1.0 equiv), MeCN, rt, 3 h. (b) **1** (ca. 1 equiv), CH_2Br_2 (1.0 equiv), 1,3,5-trimethoxybenzene (1.0 equiv as an internal standard), benzene-d_6, rt.

Further investigation of the reactivity of **3a** revealed that a methyl group in complex **4**, which was generated *in situ* by the reaction of **3a** with MeMgBr, was transferred to TEMPO under photoirradiation to afford TEMPO-Me (**Scheme 3**). In contrast, only trace amounts of TEMPO-Me were observed under dark conditions. This photo-induced reactivity of the C–Ni bond is particularly significant for the potential application of our nickel complexes in catalysis.

Scheme 3 Photo-induced methyl-transfer reaction.

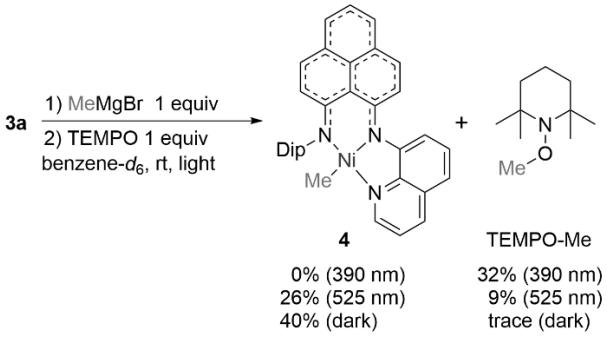

3.3. Conclusion

In conclusion, we have synthesized and characterized cationic nickel(II) complexes bearing the DipQN-PLY ligand, providing insights into their structures, electronic properties, and reactivities. The introduction of a positive charge was shown to significantly alter the electronic properties of the nickel center, as evidenced by a larger HOMO–LUMO energy gap, bathochromic shifts in the absorption spectrum, and more positive reduction potentials compared to their neutral counterparts. Reactivity studies highlighted the photo induced methyl group transfer capability of the cationic complex, demonstrating its potential for catalytic applications. These findings not only deepen our understanding of the DipQN-PLY ligand system but also underscore the versatility of cationic nickel complexes for future developments in catalysis and synthetic chemistry.

3.4. Experimental Section

I. General Information.

^{1}H, ^{13}C NMR and ^{19}F NMR spectra were recorded on a JEOL ESZ-400S spectrometer. The chemical shifts were recorded relative to MeCN (δ: 1.94 for ^{1}H NMR in CD_3CN), benzene (δ: 7.16 for ^{1}H NMR in benzene-d_6), CD_3CN (δ: 1.32 for ^{13}C NMR in CD_3CN) and C_6F_6 (δ: –165.2 for ^{19}F NMR in CD_3CN)[14] as an internal or external standard. Data are recorded as follows: chemical shifts in ppm (δ), multiplicity (s = singlet, d = doublet, brs = broad singlet, m = multiplet), coupling constant (Hz), and integration. Infrared spectra (IR) were obtained using a JASCO FT/IR-4200 spectrometer. Absorption is reported in reciprocal centimeters (cm^{-1}) with the following relative intensities: s (strong), m (medium), or w (weak). High resolution mass spectra (HRMS) were obtained using a JEOL JMS-T100LP spectrometer. Elemental analyses were performed on a J-Science Lab. Co. MICRO CORDER JM10 elemental analyzer. Melting points were determined on a BUCHI melting point M-565 and are uncorrected. Electronic absorption spectra were recorded on a JASCO V-770 spectrophotometer and an Agilent 8453 UV–vis spectroscopy system. Cyclic voltammograms were recorded at room temperature using an EC Frontier ECstat-302 electrochemical analyzer. Two kinds of light source were used in this work (52 W purple LED, Kessil PR160L 390 nm LED, 370–410 nm), (44 W green LED, Kessil PR160L 525 nm LED, 490–570 nm). These light sources were used at 100% intensity at 5.0 cm far from the samples.

II. Materials.

All commercially available reagents and solvents were supplied from TCI, WAKO and Aldrich. 2^4, 4^4 and K-DipQN-PLY[4] were prepared according to a literature procedure. All reactions with moisture- or air-sensitive compounds were performed in a nitrogen- and argon-filled glove box.

III. Synthesis of nickel complexes.

Synthesis of 3a. K-DipQN-PLY (1.1 g, 2.0 mmol) and $Ni(OTf)_2$ (0.71 g, 2.0 mmol) were placed in a Schlenk, and toluene (32 mL) was added. The color of the reaction mixture turned to brown after the mixture was stirred for 15 h at 65 °C. Then, the MeCN (10 mL) was added to the crude mixture, and the mixture was stirred at rt for changing the color from brown to dark-red. After the color change was completed, hexane (10 mL) was added and kept silent for reprecipitation of KOTf. Appearing precipitation, the residue was filtered off to obtain dark-red solution and insoluble

dark-gray powder. Then, the solution was evaporated, and obtained solid was re-solved with MeCN (10 mL) to precipitate. After residue was coming from the solution, the mixture was filtered off and obtained filtrate was evaporated. Then, the resulting solid was re-solved with MeCN and toluene, and the mixture was evaporated to remove excess MeCN. After evaporation and drying, dark-red powder was obtained (53 %, 0.78 g, 1.0 mmol).

Mp >300 °C.

^{1}H NMR (CD_3CN, 400 MHz) δ: 8.59 (brs, 1H), 8.37 (brs, 1H), 8.18–7.98 (m, 4H), 7.83 (brs, 1H), 7.76–7.73 (m, 5H), 7.38 (brs, 3H), 6.65 (brs, 1H), 3.73 (brs, 2H), 1.57 (brs, 6H), 1.07 (brs, 6H).

These signals were broadened by the insolubility of the compound to the organic solvents.

^{13}C NMR (CD_3CN, 101 MHz) δ: 156.0, 152.1, 148.2, 147.4, 144.2, 144.1, 141.6, 141.4, 136.8, 136.7, 135.3, 132.0, 131.7, 130.4, 129.6, 128.0, 127.6, 127.2, 125.5, 125.1, 124.7, 124.6, 123.6, 122.6, 122.0, 116.8, 29.5, 24.5, 24.1.

^{19}F NMR (CD_3CN, 379 MHz) δ: –79.8.

IR (KBr, cm^{-1}): 3438 w, 3060 w, 2963 m, 2929 m, 2870 w, 2326 w, 2300 w, 2218 w, 1934 w, 1626 m, 1577 m, 1486 m, 1426 w, 1382 w, 1333 m, 1252 s, 1159 s, 1100 w, 1031 s, 967 w, 845 w, 818 w, 770 m, 697 w, 639 s, 576 w, 519 m, 497 w, 449 w.

HRMS (ESI+ in MeCN) m/z $[M+MeCN]^+$ Calcd for $C_{36}H_{33}N_4{}^{58}Ni^+$; 579.20532, found: 579.20477.

Elemental Anal. Calcd for $C_{37}H_{33}N_4NiSO_3F_3$: C, 60.92; H, 45.6; N, 7.68. Found: C, 60.92; H, 4.56; N, 7.10.

Reactivity of 3a.

Complex **3a** (146.0 mg, 0.20 mol) and Cp^*_2Co (66.6 mg, 0.20 mol) were added to MeCN (10 mL) and the mixture was stirred at room temperature for 3 h under argon atmosphere. The resulting mixture was evaporated and the resulting residue was washed with toluene until no color solvent appeared. Then the resulting filtrate was evaporated and dried under reduced pressure to give a desired product **3a** as a dark red solid (97.6 mg).

Generation of **3a** was identified by ESR(**Figure S1**), UV-vis spectroscopy(**Figure S2**) and HRMS.[4]

HRMS (ESI in MeCN) *m/z* $[M+H]^+$ Calcd for $C_{34}H_{31}N_3{}^{58}Ni^+$: 539.1866, found: 539.1842.

Figure S1 ESR spectrum of this work (solid) and previous work[4] (dotted).

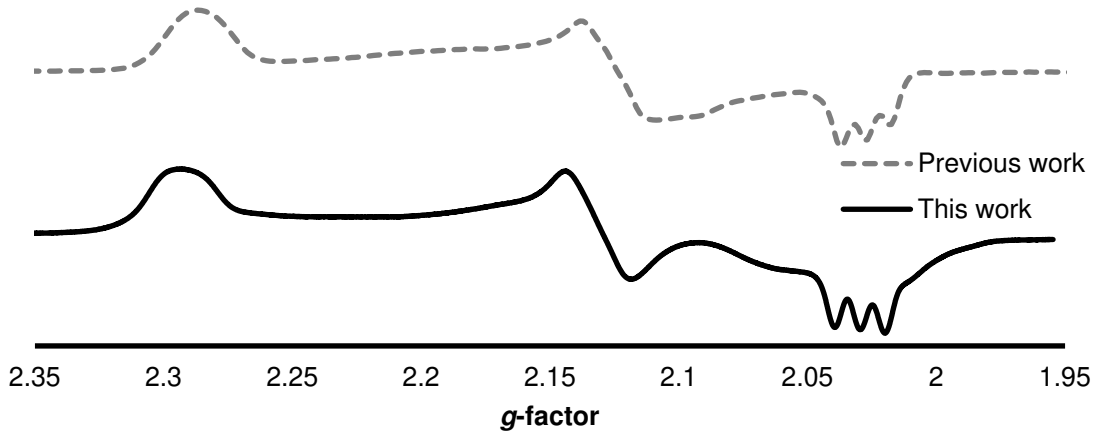

Figure S2 Electronic absorption spectrum of this work (solid) and previous work[4] (dotted).

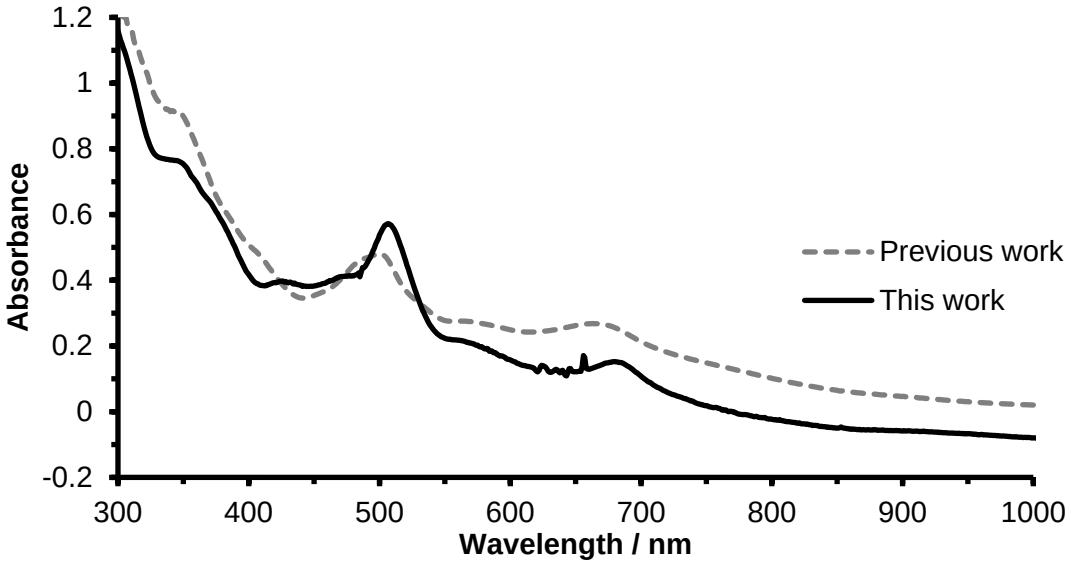

Then, part of resulting solid (5.4 mg, ca 0.01 mmol) was dissolved with benzene-d_6 (0.3 mL), and benzene-d_6 solution of CH_2Br_2 (0.1 M, 0.1 mL) and 1,3,5-trimethoxybenzene (0.1 M, 0.1 mL as an internal standard for ^{1}H NMR) were added to the solution. The mixture's color was immediately changed from dark reddish brown to dark green. The yield of **2** was determined by ^{1}H NMR.

IV. Photo-involved methyl-transfer reaction.

MeMgBr (0.05 mL, 0.015 mmol, 3 M in THF) was added to the benzene-d_6 solution of complex **3a** (9.8 mg, 0.013 mol). After 10 minutes stirring, TEMPO (3.0 mg, 0.0192 mmol) was added to the mixture, and the solution was transferred to J-young NMR tube divided into three portions. Each tubes were measured ^{1}H NMR to determine that the reaction was not occurred. Then, two of these tubes were irradiated visible light (390 nm and 525 nm of LED) and one of them was kept silent in dark. After 14 h for irradiation, 1,3,5-trimethoxybenzene (0.1 mL, 0.39 M in benzene-d_6), as an internal standard, was added to each tube and measured ^{1}H NMR. TEMPO-Me, **3a** and **4** were determined, and other byproducts were not recognized.

V Electronic Absorption Spectra.

10 mm quartz cell equipped with ground glass stopper or screw cap in a glove box was using for measurement. Electronic absorption spectra measurements for **2**, **3a** and **4** were recorded in toluene (1.0×10^{-4} M) at 25 °C.

VI. Cyclic voltammograms.

1×10^{-3} M solution of **2**(THF) and **3a**(MeCN) were prepared for measurement with 1×10^{-1} M of ^{n}Bu$_4$PF$_6$ as an electrolyte. Each measurement was two cycles from 0 V to −2 V to 1 V cycle at a scan rate of 100 mV/s with using sealed cell packed under argon atmosphere.

Fig. S3 Electronic absorption spectra of **4**.

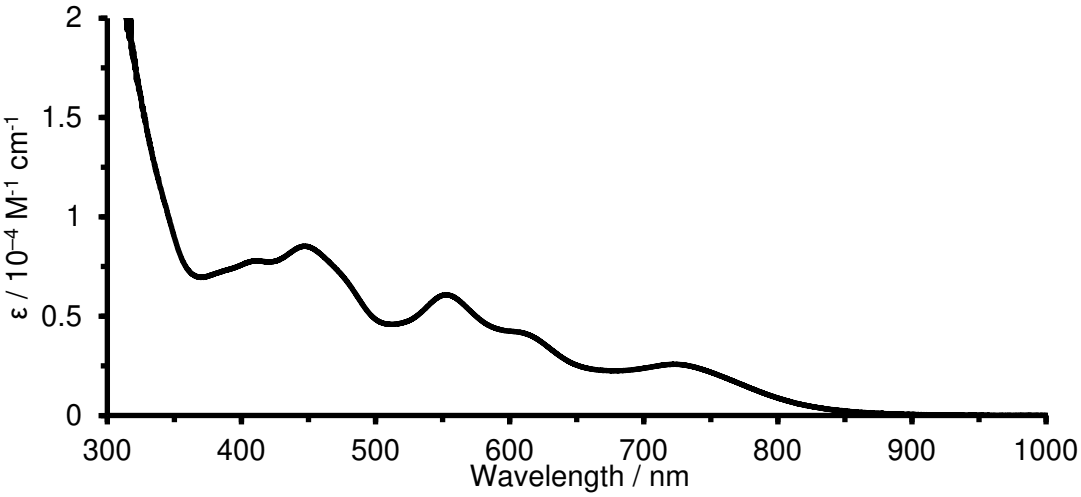

VII. Computational Details

All calculations were conducted using the Gaussian 16 (G16 Rev C.01).[15] Optimization and NPA were performed at the (U)M06/def2TZVPP level of theory. Harmonic vibration frequency analysis was conducted with the optimized structures at the same level of theory to verify all stationary points as local minima (with no imaginary frequency). Each reported minimum has no imaginary frequency. All structures, orbitals and spin density maps were visualized by GaussView 6.1.1[16] and Chemcraft Version 1.8[17].

Table S1 Selected structural parameters of **2** and **3b.**

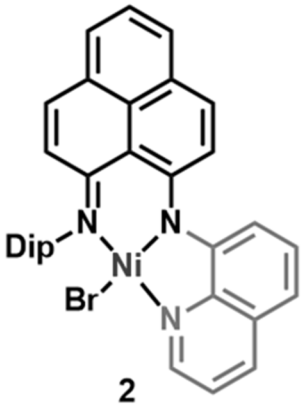

NiBr	Length(Å)
N1–Ni	1.903(5)
N2–Ni	1.870(5)
N3–Ni	1.939(5)
Br–Ni	2.330(1)
NiBr	**Angle(°)**
N1–Ni–N3	173.4(2)
N2–Ni–Br	173.5(2)

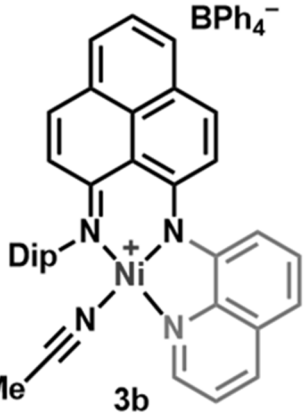

Ni⁺	Length(Å)
N1–Ni	1.879(2)
N2–Ni	1.852(2)
N3–Ni	1.918(2)
N4–Ni	1.902(2)
Ni⁺	**Angle(°)**
N1–Ni–N3	173.83(7)
N2–Ni–N4	175.54(7)

VIII. Cartesian Coordinates and Energies of Optimized Structures

3 (cationic part)

N	-2.87766700	-0.64679100	-0.77673100	H	2.80615000	1.69237700	1.11728800
N	-0.61612600	-1.63436000	-0.08532700	C	-2.94577900	-1.89058500	-0.23398200
N	0.58748900	0.75683700	0.05114800	C	0.79660300	-3.48931200	-0.70401000
C	0.00954900	3.81158300	2.04821000	H	-0.08178000	-4.06317500	-0.96088900
H	-0.38203100	4.09460800	3.01803400	C	-1.71638700	-2.43758300	0.18437600
C	2.87867700	0.67877400	0.75006300	C	1.69172300	0.04666300	0.24183500

C	0.43541300	4.79423800	1.17491000	H	-6.09133400	-0.23776300	-1.58535500
H	0.37588600	5.83694500	1.46044800	C	5.59294400	-3.19894100	-0.24820500
C	2.02280300	-4.04071500	-0.85118400	H	6.56711900	-3.66554400	-0.29868600
H	2.11861900	-5.05542900	-1.22028500	C	4.07624400	0.05932300	0.72786200
C	3.10681400	3.18290900	-1.87612100	H	4.95756000	0.58147400	1.08359700
H	3.21288600	4.26817300	-1.81494200	C	4.22490100	-1.26755900	0.24418500
H	3.54294900	2.86314800	-2.82357400	C	-1.74730100	-3.64029500	0.85791800
H	3.69435600	2.74372300	-1.06905200	H	-0.83611600	-4.06526200	1.25599400
C	3.05758400	-1.97106900	-0.13008200	C	4.46246000	-3.90493700	-0.59770100
C	3.19531100	-3.31930900	-0.52820700	H	4.53988200	-4.93519500	-0.92505400
C	0.62464500	-2.14115700	-0.27287400	C	-2.95953000	-4.32365800	1.04177300
C	1.77880400	-1.34972400	-0.07684400	H	-2.94397600	-5.26686200	1.57220100
C	0.09725700	2.46583100	1.71233600	C	-0.35236800	1.40938600	2.69664300
C	-3.98042000	-0.09644000	-1.24141800	H	-0.00016200	0.43966400	2.33520400
H	-3.89413400	0.88815300	-1.67953100	C	5.46702600	-1.88952000	0.18512100
C	0.59745500	2.13125400	0.44856400	H	6.34343100	-1.33033100	0.49166900
C	1.05191700	3.11001800	-0.44570800	C	-1.87331200	1.34278400	2.77499400
C	0.96337400	4.44039800	-0.05354800	H	-2.28779200	2.29555400	3.11408300
H	1.32461000	5.21584000	-0.72014100	H	-2.19013800	0.57209400	3.47984100
C	-4.14450300	-3.83255800	0.56868600	H	-2.31924400	1.11178700	1.80261100
H	-5.07131100	-4.37471900	0.70354300	C	0.24924700	1.62162400	4.07843200
C	0.86249200	3.39674200	-2.94629100	H	1.33663000	1.69972600	4.03077500
H	0.85646300	4.48716600	-2.87653100	H	-0.00198400	0.78517100	4.73192700
H	-0.17160500	3.04797700	-2.97690200	H	-0.13145400	2.52790300	4.55327800
H	1.32140900	3.13683000	-3.90120800	Ni	-1.11155300	0.10810700	-0.47954100
C	1.64126600	2.76810200	-1.79676100	N	-1.74573800	1.84219100	-0.94425200
H	1.59124500	1.68422100	-1.92332700	C	-2.08584300	2.91859300	-1.12610800
C	-4.16099700	-2.58475700	-0.08310200	C	-2.47108800	4.28641800	-1.34785200
C	-5.31552500	-1.96440200	-0.58879900	H	-1.61643000	4.92765300	-1.12602700
H	-6.27054700	-2.46906100	-0.50297400	H	-2.77028500	4.43192100	-2.38548300
C	-5.22194800	-0.73512200	-1.17955800	H	-3.29813500	4.55711900	-0.69254400

Method: M06/def2TZVPP opt freq

imaginary frequencies: 0

EE + Thermal Free Energy Correction: − 3117.775922 Hartree

2

Br	-1.40826100	-2.37696600	-1.45540500	C	2.71388300	3.74607400	-0.59866600
Ni	-1.03376000	-0.26888000	-0.52118400	C	2.94599100	-0.17984200	0.90870400
N	0.74235300	-0.65832600	0.07847700	H	3.00308600	-1.16332900	1.35263500
N	-2.92188200	0.22967800	-0.70877300	C	1.44943300	4.28482600	-0.93797000
N	-0.81290200	1.55061900	-0.07270100	H	1.40189900	5.28866300	-1.34532600
C	-5.27354500	-0.03403400	-0.97955100	C	0.42505300	-2.30426200	1.83577000
H	-6.07582800	-0.66387200	-1.33774400	C	-3.95265700	-0.48101000	-1.11464400
C	0.33514500	2.22554800	-0.28032200	H	-3.72292100	-1.44532600	-1.55091300
C	3.76565100	-2.56869300	-1.47627900	C	0.94708800	-1.98870900	0.57677100
H	4.17199300	-3.53924200	-1.18013700	C	1.82641200	-3.63289100	-2.60606200
H	4.12457000	-1.82478000	-0.76524100	H	2.19297100	-3.31276600	-3.58341100
H	4.17849400	-2.32405300	-2.45716500	H	0.74329900	-3.73091500	-2.65947900
C	-5.52312300	1.16687700	-0.38334900	H	2.25452600	-4.61852000	-2.40854900
H	-6.53682900	1.52474200	-0.24421900	C	4.03767000	0.60500200	0.87413700

H	4.97043700	0.24824700	1.29773600	C	-2.18769000	3.37480600	0.89267200
C	0.58154500	-3.60048700	2.30861800	H	-1.33245400	3.93130000	1.25125800
H	0.16958000	-3.86818600	3.27483100	C	2.24153500	-2.62489800	-1.54119900
C	-2.00260700	2.18014700	0.22347800	H	1.87163100	-1.64497400	-1.85343400
C	0.31511200	3.57513500	-0.75122600	C	1.78814000	-4.21133700	0.34093700
H	-0.64029900	4.00884600	-1.01089100	H	2.32045100	-4.96132000	-0.23223000
C	1.64328200	-2.93545800	-0.18603800	C	5.10101100	3.97908500	-0.30427900
C	-3.15289100	1.44788500	-0.14841200	H	6.00113900	4.57481000	-0.37599800
C	1.58974700	1.61114600	-0.07417900	C	-4.59330900	3.19619900	0.71376000
C	-4.44828500	1.95495600	0.06387800	H	-5.58653400	3.58843800	0.89183400
C	2.76431700	2.40831200	-0.14257700	C	-0.31991900	-1.28762900	2.67164600
C	1.70005200	0.22093700	0.29597800	H	-0.17703100	-0.30399600	2.21732400
C	3.88664600	4.50002500	-0.69349400	C	0.21562200	-1.20416000	4.09369000
H	3.82001500	5.51462300	-1.06978000	H	0.04494300	-2.13080300	4.64589300
C	1.25687200	-4.55077000	1.56990400	H	-0.28485700	-0.40301500	4.64118100
H	1.37195600	-5.55711900	1.95256800	H	1.28881500	-1.00344100	4.10279900
C	4.01380400	1.90348300	0.28979800	C	-1.81683400	-1.57630600	2.66956200
C	-3.47784800	3.86938000	1.12905200	H	-2.20763200	-1.63511600	1.65036700
H	-3.58319100	4.80931100	1.65614000	H	-2.36193600	-0.79638200	3.20697500
C	5.15382000	2.69035300	0.20553000	H	-2.02800600	-2.53177500	3.15654600
H	6.09440500	2.28046100	0.55590600				

Method: UM06/def2TZVPP opt freq

imaginary frequencies: 0

EE + Thermal Free Energy Correction: − 5559.381525 Hartree

1

Ni	-1.07303300	0.63349900	-0.34961600	C	1.28728600	-1.55588800	-0.00818800
N	-2.98850300	0.50589200	-0.54877300	C	1.05212200	2.79930900	1.39486500
N	-1.12582900	-1.27926400	-0.00041600	C	-3.86847700	1.42425900	-0.88465300
N	0.75120600	0.82631000	-0.00612000	H	-3.47137800	2.38605700	-1.19068100
C	1.33080700	4.15595800	1.48699600	C	1.11985300	2.18844200	0.13361800
H	1.27626100	4.64469500	2.45302700	C	1.47080400	2.92453500	-1.00747100
C	2.98878700	0.18368700	0.46763900	C	1.73851200	4.27913800	-0.86449400
H	3.21747500	1.22531700	0.65142900	H	2.00469300	4.86359900	-1.73752300
C	-3.42125900	-0.72038800	-0.14349100	C	-5.19350700	-2.25468100	0.50767400
C	-0.20558700	-3.43369200	-0.53680400	H	-6.24839600	-2.47575600	0.61043800
H	-1.19700800	-3.77057300	-0.80283600	C	0.15554000	2.52953800	-3.07378100
C	-2.41945800	-1.69272800	0.18571500	H	0.00407800	3.60125100	-3.22867800
C	1.62211300	-0.15159600	0.15675800	H	-0.68327900	2.15170200	-2.47683800
C	1.67193100	4.89572300	0.37046100	H	0.12353600	2.03634300	-4.04745800
H	1.88614500	5.95301700	0.46299300	C	1.48457800	2.27550100	-2.37077800
C	0.83106500	-4.28980900	-0.61698900	H	1.57984600	1.19674900	-2.22568000
H	0.67085400	-5.31663700	-0.92743400	C	-4.79566600	-1.00906300	-0.01542900
C	2.64753600	2.72478800	-3.24034300	C	-5.70655400	-0.00731900	-0.39931200
H	2.56441000	3.77709000	-3.52149600	H	-6.76915900	-0.20866600	-0.32614200
H	2.67118700	2.14635000	-4.16554100	C	-5.24890900	1.19976000	-0.84322700
H	3.60241700	2.58796400	-2.72966800	H	-5.92707900	1.98751300	-1.14052200
C	2.36399300	-2.49636200	-0.02736700	C	4.49771700	-4.37307100	-0.04587400
C	2.14728300	-3.86950600	-0.30999000	H	5.31146900	-5.08590900	-0.05137000
C	-0.05100400	-2.06134000	-0.15341900	C	3.96702000	-0.73579900	0.50899800

H	4.98558900	-0.44064600	0.73667800	C	4.73309200	-3.03847500	0.23315500
C	3.70316900	-2.10509100	0.23611300	H	5.73792500	-2.69485000	0.45233700
C	-2.86870900	-2.87379900	0.75596600	C	-0.84229000	2.29161900	2.92118700
H	-2.15272200	-3.59967500	1.11494900	H	-1.00054200	3.35014200	3.14444900
C	3.20900000	-4.77514300	-0.32155100	H	-1.17727300	1.70969000	3.78233800
H	2.99554800	-5.81248000	-0.55434000	H	-1.47207100	2.02738300	2.06604400
C	-4.23500400	-3.14308300	0.90745900	C	1.49421600	2.30407800	3.83364900
H	-4.52882900	-4.08610000	1.35191500	H	2.55176700	2.14440200	3.61462100
C	0.62667800	2.02064800	2.61746700	H	1.21533000	1.64533700	4.65799900
H	0.71951700	0.95648100	2.38848900	H	1.37643200	3.33077900	4.18757000

Method: UM06/def2TZVPP opt freq

imaginary frequencies: 0

EE + Thermal Free Energy Correction: − 2985.261411 Hartree

3.5. References

1. Selected reviews on cationic transition metal complexes, see; (a) Mecking, S. *Coord. Chem. Rev*. **2000**, *203*, 325. (b) Wu, R.; Wu, W. K.; Stieglitz, L.; Gaan, S.; Rieger, B.; Heuberger, M. *Coord. Chem. Rev.* **2003**, *474*, 214844.

2. Boniolo, M.; Chernev, P.; Cheah, M. H.; Heizmann, P. A.; Huang, P.; Shylin, S. I.; Salhi, N.; Hossain, M. K.; Gupta, A. K.; Messinger, J.; Thapper, A.; Lundberg, M. *Dalton Trans.* **2021**, *50*, 660.

3. Selected reviews on Ni(I) complex, see; (a) Lin, C.-Y.; Power, P. P.; *Chem. Soc. Rev*. **2017**, *46*, 5347. (b) Diccianni, J.; Lin, Q.; Diao, T. *Acc. Chem. Res.* **2020**, *53*, 906. (c) Day, C. S.; Rentería-Gómez, Á.; Ton, S. J.; Gogoi, A. R.; Gutierrez, O.; Martin, R. *Nat. Catal*. **2023**, *6*, 244. (d) Day, C. S.; Martin, R. *Chem. Soc. Rev.* **2023**, *52*, 6601. (e) Dawson, G. A.; Spielvogel, E. H.; Diao, T. *Acc. Chem. Res.* **2023**, *56*, 3640.

4. Noguchi, H.; Kodama, T.; Kikkawa, S.; Yamazoe, S.; Tobisu, M. *Chem. Lett.* **2024**, *53*, upae236.

5. (a) Mukherjee, A.; Sau, S. C.; Mandal, S. K. *Acc. Chem. Res.* **2017**, *50*, 1679. (b) Ahmed, J.; Mandal, S. K. *Chem. Rev.* **2022**, *122*, 11369.

6. Related phenalenyl-based bidentate ligand system was reported, see; (a) Kodama, T.; Mukai, N.; Tobisu, M. *Inorg. Chem*. **2023**, *62*, 6554. (b) Kodama, T.; Uchida, K.; Nakasuji, C.; Kishi, R.; Kitagawa, Y.; Tobisu, M. *Inorg. Chem*. **2023**, *62*, 7861.

7. Selected examples for metalloradicals, see; (a) Ingleson, M. J.; Fullmer, B. C.; Buschhorn, D. T.; Fan, H.; Pink, M.; Huffman, J. C.; Caulton, K. G. *Inorg. Chem.* **2008**, *47*, 407. (b) Rettenmeier, C.; Wadepohl, H.; Gade, L. H. *Chem. Eur. J*. **2014**, *20*, 9657. (c) Yoo, C.; Lee, Y. *Angew. Chem., Int. Ed*. **2017**, *56*, 9502. (d) Schneck, F.; Ahrens, J.; Finger, M.; Stueckl, A. C.; Wuertele, C.; Schwarzer, D.; Schneider, S. *Nat. Commun*. **2018**, *9*, 1161. (e). Ghannam, J.; Sun, Z.; Cundari , T. R.; Zeller, M.; Lugosan, A.; Stanek, C. M.; Lee, W.-T. *Inorg. Chem.* **2019**, *58*, 7131. (f) Duan, P.-C.; Schulz, R. A.; Römer, A.; Van Kuiken, B. E.; Dechert, S.; Demeshko, S.; Cutsail III, G. E.; DeBeer, S.; Mata, R. A.; Meyer, F. *Angew. Chem., Int. Ed*. **2021**, *60*, 1891. (g) Pahar, S.; Sharma, V.; Raj, K. V.; Sangole, M. P.; George, C. P.; Singh, K.; Vanka, K.; Gonnade, R. G.; Sen, S. S. *Chem. Eur. J*. **2024**, *30*, e202303957.

8. Kodama, T.; Noguchi, H.; Tsurugi, H.; Tobisu, M. *Chem. Lett.* **2024**. DOI: 10.1093/chemle/upae246

9. We confirmed that reaction of **2** with $AgPF_6$ can be converted to the PF_6 analogue of **3**, although it was difficult to remove inorganic impurities

10. Zhao, Y.; Truhlar, D. G. *Theor. Chem. Acc*. **2008**, *120*, 215.

11. (a) Weigend, F.; Ahlrichs, R. *Phys. Chem. Chem. Phys*. **2005**, *7*, 3297. (b) Weigend, F. *Phys. Chem. Chem. Phys.* **2006**, *8*, 1057. (c) Zheng, J.; Xu, X.; Truhlar, D. G. *Theor. Chem. Acc*. **2011**, *128*, 295.
12. Martin, R. L. *J. Chem. Phys.* **2003**, *118*, 4775.
13. Connelly, N. G.; Geiger, W. E. *Chem. Rev.* **1996**, *96*, 877.
14. Lee, G. M.; Harrison, D. J.; Korobkov, I.; Tom, R. B. *Chem. Commun.* **2014**, *50*, 1128.
15. Frisch, M. J.; Trucks, G. W.; Schlegel, H. B.; Scuseria, G. E.; Robb, M. A.; Cheeseman, J. R.: Scalmani, G.; Barone, V.; Mennucci, B.; Petersson, G. A.; Nakatsuji, H.; Caricato, M.; Li, X.; Hratchian, H. P.; Izmaylov, A. F.; Bloino, J.; Zheng, G.; Sonnenberg, J. L.; Hada, M.; Ehara, M.; Toyota, K.; Fukuda, R.; Hasegawa, J.; Ishida, M.; Nakajima, T.; Honda, Y.; Kitao, O.; Nakai, H.; Vreven, T.; Montgomery, Jr., J. A.; Peralta, J. E.; Ogliaro, F.; Bearpark, M.; Heyd, J. J.; Brothers, E.; Kudin, K. N.; Staroverov, V. N.; Keith, T.; Kobayashi, R.; Normand, J.; Raghavachari, K.; Rendell, A.; Burant, J. C.; Iyengar, S. S.; Tomasi, J.; Cossi, M.; Rega, N.; Millam, J. M.; Klene, M.; Knox, J. E.; Cross, J. B.; Bakken, V.; Adamo, C.; Jaramillo, J.; Gomperts, R.; Stratmann, R. E.; Yazyev, O.; Austin, A. J.; Cammi, R.; Pomelli, C.; Ochterski, J. W.; Martin, R. L.; Morokuma, K.; Zakrzewski, V. G.; Voth, G. A.; Salvador, P.; Dannenberg, J. J.; Dapprich, S.; Daniels, A. D.; Farkas, O.; Foresman, J. B.; Ortiz, J. V.; Cioslowski, J.; Fox, D. J. Gaussian, Inc., Wallingford CT, **2016**.
16. Dennington, R.; Keith, T. A.; Millam, J. M.; Semichem Inc., Shawnee Mission, KS, **2016**.
17. G. A. Andirenko, https://www.chemcraftprog.com.

Conclusion

The research described in this thesis focuses on the synthesis and properties of a T-shaped nickel metalloradicals.

In chapter 1, the author synthesized a new PLY-based N,N,N-tridentate ligand and corresponding alkali metal salts, and investigated their spectroscopic properties UV-vis spectroscopy revealed that both free ligand and alkali metal salts can absorb visible light, and complexation of alkali metal salts caused bathochromic shift compared with its free ligand. DFT calculated optimization suggested that the ligand structure was distorted by complexation and the degree of distortion increased with increasing ionic radii of alkali metals. Given the successful complexation even with large cesium ion, the author believes that the ligand system is applied to some other metals bigger than nickel.

In chapter 2, the author synthesized the T-shaped nickel metalloradical using the ligand developed in chapter 1. Spectroscopic investigations revealed successful synthesis of the metalloradical. UV-vis spectroscopy and DFT studies showed the MLCT absorption, which is one of the features of the metalloradical. Furthermore, XAFS and ESR measurements in solution state suggested that the obtained complex has certain characters of T-shaped nickel metalloradical. In addition, the complex has typical reactivity of metalloradical, such as halogen abstraction and homolytic cleavage of weak covalent bonds.

In chapter 3, the author developed other pathways to synthesize the metalloradical. In chapter 2, potassium hydride, which is a strong reductant and flammable in air, was needed to reduce Ni–Br bond. This issue was overcome by using a cationic complex without bromo moiety on nickel. X-ray crystallography revealed that T-shaped geometry remained after removing the bromo group. In addition, the author found that Ni–Me complex can release methyl radical under blue LED irradiation. It indicated that photolysis of Ni–Me complex has possibilities to provide metalloradical and to promote S_H2 involving MRC.

In this thesis study, the author succeeded in synthesizing a new T-shaped nickel metalloradical. Several reductive pathways to the nickel metalloradical have been developed, including hydride reagents, single electron reductant, and photolysis of Ni–Me bond. The author believes that these findings and knowledge gained in this study will contribute to the further development of creating new types of catalytic transformation involving metalloradicals. One of the challenges in developing new types of MRC is synthesis of metalloradicals due to their instability. The author hopes that our methodology provides easier ways to new metalloradicals and following MRC. Furthermore, the ligand can be readily derived from PLY and quinolyl moieties, which is much more facile than the typical porphyrin-based system.

The author wishes that our complex and its derivatives are one of suitable complexes for metalloradical catalysis.

List of Publications

1. **Noguchi, H.**; Kodama, T.; Kikkawa, S.; Yamazoe, S.; Tobisu. M.
   A Nickel Metalloradical Bearing a Phenalenyl-Based Tridentate Ligand.
   Chem. Lett. **2024**, *53*, upae236.
2. Kodama, T.; **Noguchi, H.**; Tsurugi, H.; Tobisu. M.
   Synthesis and Characterization of Alkali Metal Salts Bearing a Phenalenyl-Based Tridentate Ligand.
   Chem. Lett. **2024**. DOI: 10.1093/chemle/upae246
3. Kodama, T.; **Noguchi, H.**; Tsurugi, H.; Tobisu. M.
   Cationic Nickel(II) Complexes Bearing a Phenalenyl-Based Tridentate Ligand.
   Chem. Lett. **2024**. DOI: 10.1093/chemle/upae251

Supplementary List of Publication

1. Umeda, M.; **Noguchi, H**.; Nishimura, T.
   Enantioselective Synthesis of Chiral Indane Derivatives by Rhodium-Catalyzed Addition of Arylboron Reagents to Substituted Indenes.
   Org. Lett. **2020**, *22*, 9597.
2. Fukumoto, Y.; Shiratani, M.; **Noguchi, H**.; Chatani, N.
   Iridium-Catalyzed Direct Amidation of Imidazoles at the C-2 Position with Isocyanates in the Presence of Hydrosilanes Leading to Imidazole-2-Carboxamides.
   Synthesis **2021**, *53*, 3011.